Design and Functions of Sheet-Shaped Macromolecules

Shun WAN

A Thesis Presented to

The Graduate University for Advanced Studies

Table of Contents

List of Tables

List of Figures

PAGE

Chapter 1

General Introductions

1-1. Covalent Organic Frameworks

Review of Covalent Organic Frameworks

Covalent organic frameworks (COFs) are porous and crystalline macromolecules with well-defined and predictable network architectures of building blocks. Compared with inorganic porous materials, COFs are unique in that they are made from light elements, tunable in skeleton and robust against air and organic solvents. From synthetic point of view, COFs are attractive motifs for the development of designable porous and functional macromolecular materials since they allow, upon topologically flexible design, a total elaborate control over structure parameters including composition and porosity.

Library of Covalent Organic Frameworks

In 2005, Yaghi *et al*. reported the first example of covalent organic frameworks (COFs)[1]. In Yaghi's system, the building blocks for COFs were 1,4-benzenediboronic acid (BDBA) and hexahydroxytriphenylene (HHTP). Under carefully selected reaction conditions, BDBA reacts with itself, and the boronic acid moieties condense to planar boroxine rings (Scheme 1-1)[1].

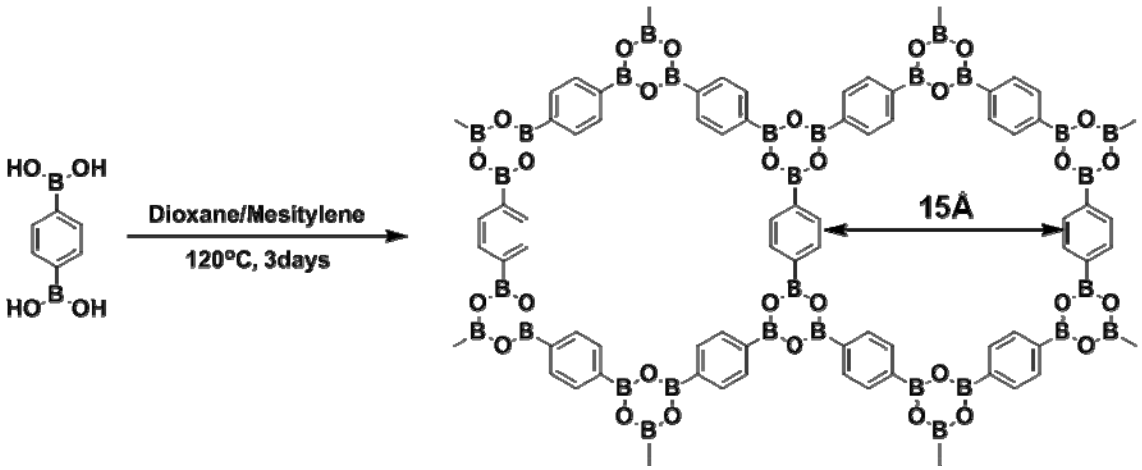

Scheme 1-1.Synthesis of the first example of covalent organic framework, COF-1.

For synthesis of COFs, it seems very important to select proper solvent. In order to form a uniform and highly ordered structure, solvents are chosen wherein the reactants are poorly soluble. Poor solvents will slow down the reversible condensation. Furthermore, the reactions are carried out in sealed pyrex tubes, again to slow down the reversible process and minimize defects by self-healing.

COF-1 was isolated as a microcrystalline substance in high yield. Powder X-ray diffraction patterns reveal a high structural order, whereas single interlayer is stacked in a staggered arrangement (Fig. 1-1A).

Solvent molecules are considered to be enclosed inside the pores and can be readily removed by heating at 200°C under vacuum without the collapse of the crystalline structure.

COF-1 has a surface area of 711 $m^2 g^{-1}$ and a pore volume of 0.32 $cm^3 g^{-1}$.

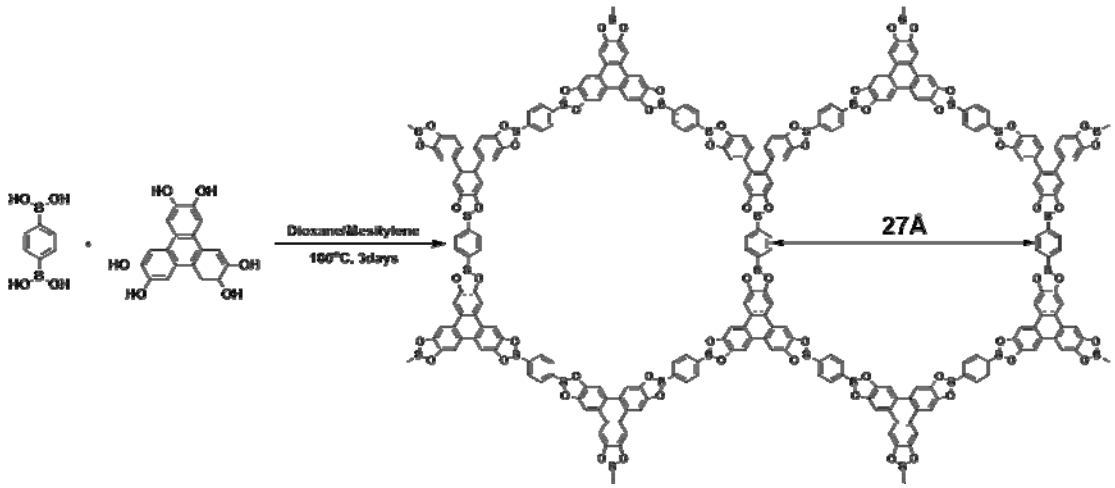

Scheme 1-2. Synthesis of COF-5.

COF-5 was also synthesized from BDBA and HHTP in high yield under similar reaction conditions (Scheme 1-2)[1]. The diameter of the pores of COF-5 is 27 Å and the pore has a narrow distribution. These data are supported by the comparison with NLDFT calculations of model compounds. The layers of the crystalline material are stacked in an eclipsed fashion (Fig. 1-1B). The specific surface area is 1590 $m^2 g^{-1}$.

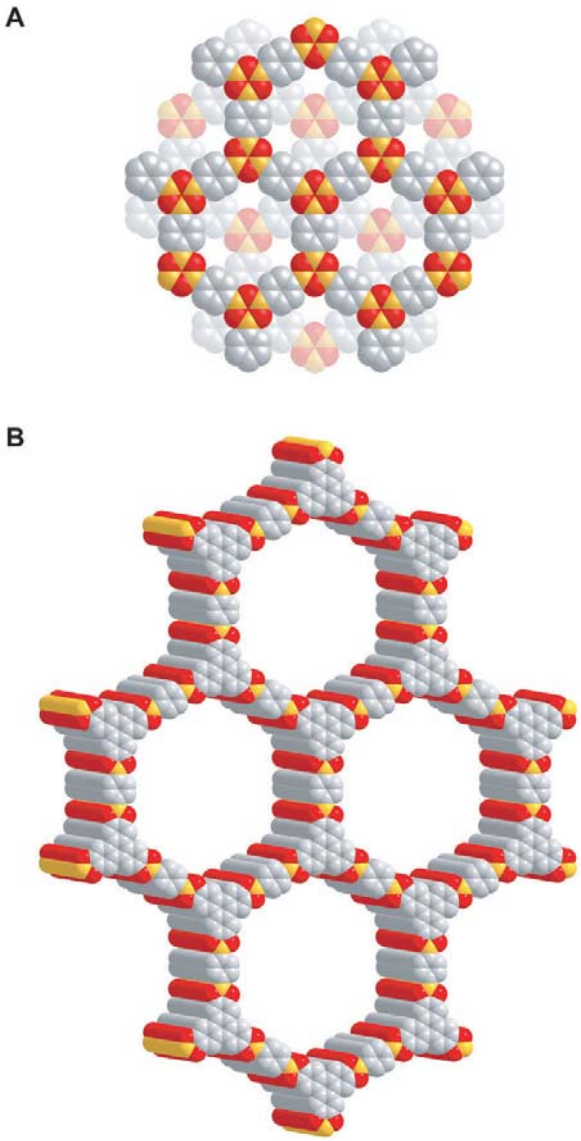

Figure 1-1.Structural representations of (A) COF-1 and (B) COF-5 based on powder diffraction and modeling projected along their c axes (H atoms are omitted). Carbon, boron, and oxygen are represented as gray, orange, and red spheres, respectively.

In 2007, Yaghi and co-workers developed co-condensation reactions of 2,3,6,7,10,11-Hexahydroxytriphenylene (HHTP) and 1,3,5-benzenetriboronic acid (BTBA), 1,3,5-benzenetris(4-phenylboronic acid) (BTPA), and 4,4-biphenyldiboronic acid (BPDA) to prepare COF-6, COF-8, and COF-10, respectively, with chemical formulas of $C_8H_3BO_2$ (COF-6), $C_{14}H_7$-BO_2 (COF-8), and C_6H_3BO (COF-10), respectively[2]. Different from previous reactions, these reactions were carried out in

glass vials using 1:1 (vol/vol) mixture of mesitylene/dioxane at 85 °C for 48-120 h. Yields were 65-76% based on HHTP.

Absorption of N_2 at 77 K was used to assess the porosity of the COFs. COF-6 exhibits a Type I isotherm indicative of a microporous material, while COFs-8 and COF-10 display Type IV isotherms, indicating their mesoporosity. Applying the Langmuir model to the appropriate low-pressure regions of the isotherms provided surface areas of 980, 1400, and 2080 $m^2 g^{-1}$ (1049, 968, and 976 $m^2 cm^{-3}$) for COF-6, COF-8, and COF-10, respectively. Pore volumes were estimated to be 0.32, 0.69, and 1.44 $cm^3 g^{-1}$ for COFs-6, -8, and -10, respectively.

Another representative of this material class is COF-18Å, which was synthesized by Lavigne's group upon condensation of 1,3,5-benzene- triboronic acid (BTBA) and 1,2,4,5-tetrahydroxybenzene (THB)[3].

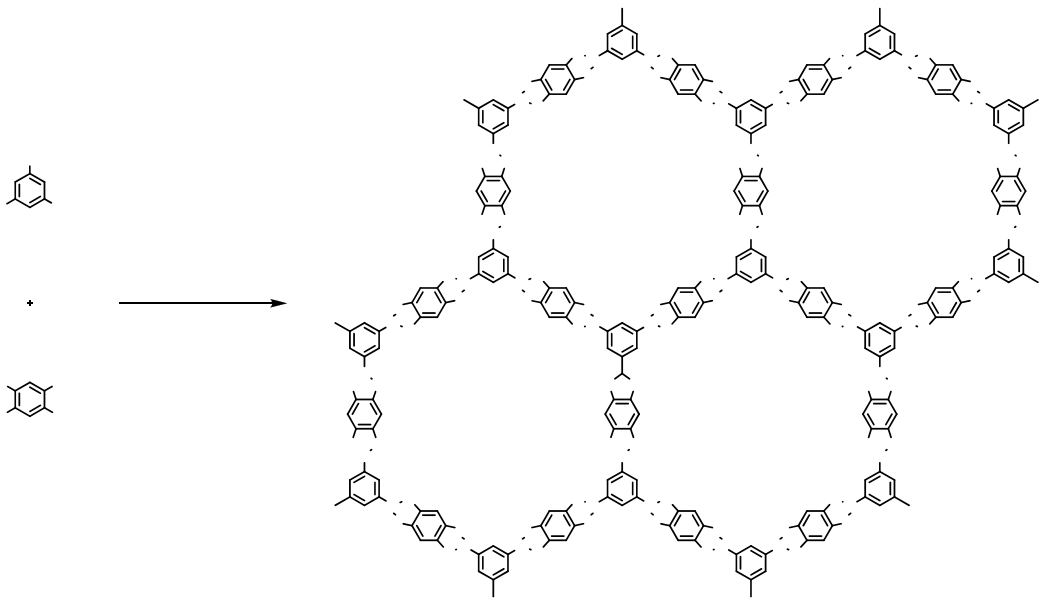

Scheme 1-3. Synthesis of COF-18Å.

Although the reaction conditions (THF/Methanol; reflux) are different from those of the Yaghi's system, COF-18Å was isolated in excellent yield (Scheme 1-3). This result confirms the concept of slow condensation as a general principle for the generation of highly ordered structures. As the name of the compound suggests, the pore diameter is 18 Å. In comparison with COF-5, COF-18Å has a smaller surface area (1260 m^2 g^{-1}) and smaller pore volumes (0.29 cm^3 g^{-1}). To verify the stoichiometric incorporation of both monomer reactants into the framework, COF-18Å was degenerated with KOH in deuterated water. A subsequently recorded by ^1H NMR spectrum reveals the expected ratio of 3:2 (BTBA/THB)[3].

Recently, Yaghi and co-workers extended the networking scope to three-dimensional space[4-5]. Using tetrahedral tetraboronic acids as precursors, 3D frameworks (COF-102, COF-103, COF-105, and COF-108) resulted from condensation or cocondensation with HHTP (Fig. 1-2 and Fig. 1-3)[4].

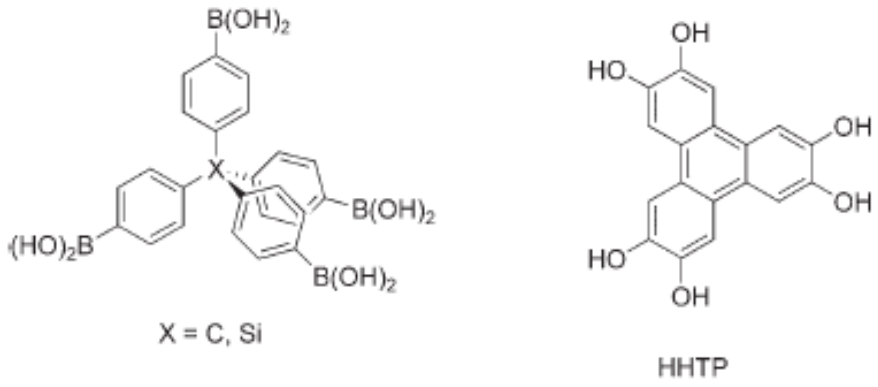

Figure 1-2.Monomeric subunits of the three dimensional COFs 102, 105, and 108.

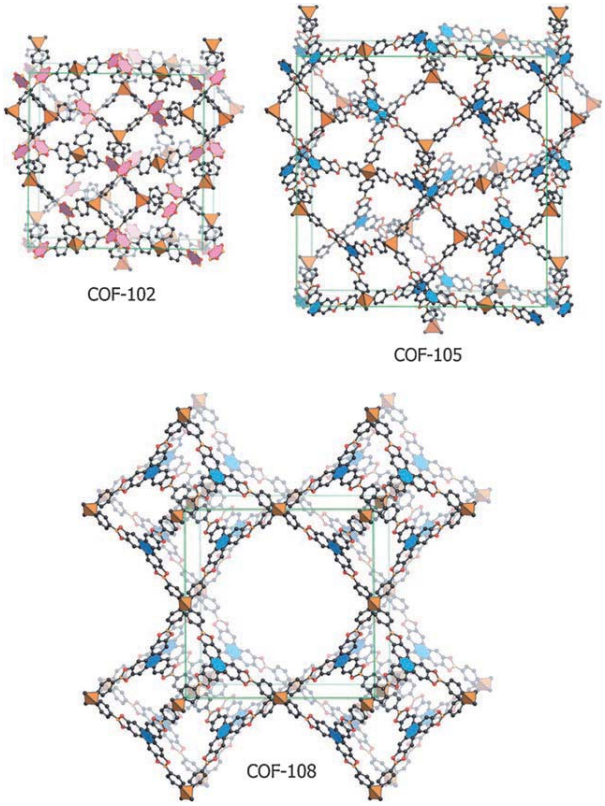

Figure 1-3.Models of the structures of COFs 102, 105, and 108.

Although the yields are lower than for the 2D frameworks, the 3D COFs display excellent physicochemical properties. The formation of two different net structures was observed: ctn and bor. Only COF-108 forms the highly porous bor network, and it is, to date, unclear why exclusively this compound crystallizes in the bor structure. The only difference from COF-105 is the central atom of the tetrahedral precursor (Si instead of C). The other three COFs condense in the ctn structure. The COFs 102, 103, and 105 exhibit pore diameters of 8.9, 9.6, and 18.3 Å and densities of 0.41, 0.38, and 0.18 g cm^{-3}, respectively. Because COF-108 crystallizes in the bor structure, two different types of pores are present, with diameters of 15.2 and 29.6 Å. With a density

of 0.17 g cm^{-3}, COF-108 is the crystalline material with the lowest density. The surface areas of COF-102 and COF-103 are 3472 and 4210 m^2 g^{-1}, respectively.

The same method of condensing diboronic acids and tetraols was also used by Lavigne and co-workers to COFs[6,7]. Recently, Lavigne and co-workers utilized triboronic acid and tetraols to build COFs[8,9]. A very similar approach of polymerization of diboronic acids with fluorene or carbazole subunits had been described by Ding and co-workers three years earlier. Dehydration of the precursor mixture led to stable crosslinked polymers. These polymers emitted blue emission and were tested as materials for organic light-emitting diodes (OLEDs)[10].

Recently, Thomas and co-workers demonstrated that it is also possible to access covalent organic frameworks with excellent porous property, which are formed from simple, cheap, and abundant aromatic nitriles[11,12].

By the dynamic trimerization reaction in ionothermal conditions[13], that is, in molten zinc chloride at high temperature, triazine-based materials with high porosities and surface areas can be obtained that are similar in performance to zeolites, metal-organic frameworks (MOFs), or the covalent boron oxide based frameworks (COFs) (Scheme 1-4).

The polymers were synthesized by heating a mixture of the nitrile and $ZnCl_2$ in quartz ampules at 400°C. The yields of these reactions are close to quantitative.

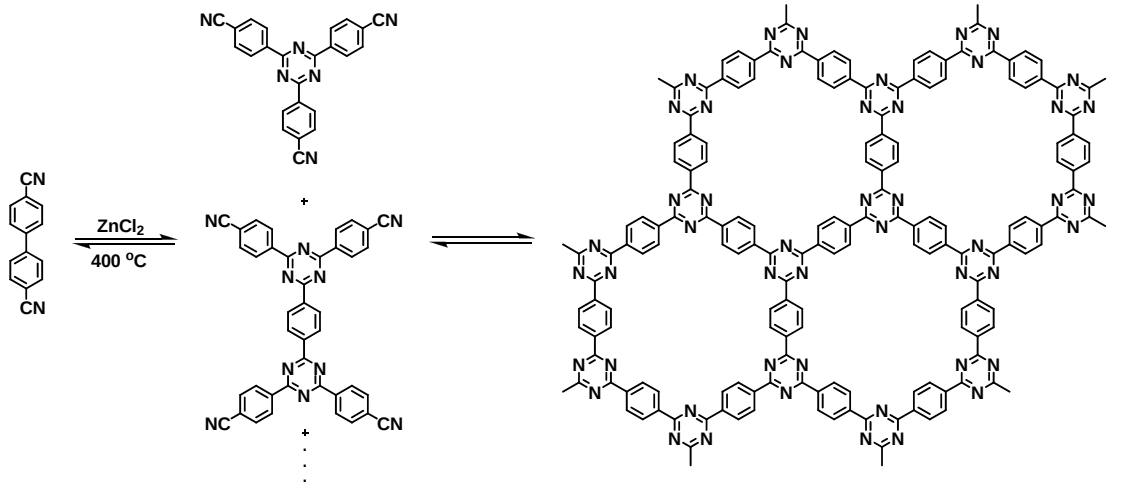

Scheme 1-4. Trimerization of dicyanobenzene in molten $ZnCl_2$ to trimers and oligomers and then to a covalent triazine-based framework (CTF-1).

As measured by nitrogen-sorption experiments, CTF-1 shows a surface area of 791 m^2 g^{-1} with a total pore volume of 0.40 cm^3 g^{-1}. These values are close to those found for COF-1 (711 m^2 g^{-1} and 0.32 cm^3 g^{-1})[1]. From the pore size distribution determined by nonlocal DFT (NLDFT), a pore size of 1.2 nm is found, which is in agreement with the pore size measured from the optimized model of CTF-1. The high thermostabilities of the COFs up to 500°C make these compounds potential candidates for use in industrial processes. The low densities and large surface areas up to 4210 m^2 g^{-1} are also properties suitable for potential applications. Above examples also demonstrate that COFs will be new exciting field of chemistry.

1-2. Scope of This Thesis

As described above, most studies up to date have mainly focused on the development of synthetic methodologies with an aim to optimize pore size and surface area. Thus, the functions of COFs except for gas storage[14,15,16] have not yet been well

explored. This motivated us to explore the possibility for constructing functional COFs with novel properties by utilizing highly ordered π-conjugation systems.

In Chapter 2, the author designed the first example of a luminescent and semiconducting COF, utilizing newly synthesized PDBA and HHTP as monomers.

In Chapter 3, the author demonstrated the synthesis of a new π-electronic COF based on self-condensation of pyrene diboronic acid under solvothermal condition (PPy-COF), whose 2D poly(pyrene) sheets align in a perfectly eclipsed fashion. Up to date, self-condensation of boronic acid derivatives has been limited to only one example, *i.e.*, benzene 1,4-diboronic acid, which leads to a COF with staggered alignment of 2D polymer sheets.

In Chapter 4, the author disclosed the design and synthesis of a new type of COF consisting of anthracene building blocks based on the co-condensation of benzene triboronic acid and 2,3,6,7-tetrahydroxy- anthracene under solvothermal or reflux conditions (An-COF).

Based on these researches, the author succeeded in open a new way to polymeric optoelectronics and electronics for large π-electronic organic frameworks.

1-3. Reference

1. A. P. Côté, A. I. Benin, N. W. Ockwig, M. O'Keeffe, A. J. Matzger, O. M. Yaghi, Science 2005, *310*, 1166-1170.

2. A. P. Côté, H. M. El-Kaderi, H. Furukawa, J. R. Hunt, O. M. Yaghi, *J. Am. Chem. Soc.*, **2007**, *129*, 12914-12915.

3. R.W. Tilford,W . R. Gemmill, H. C. zur Loye,J . J. Lavigne, *Chem. Mater.* **2006**, *18*, 5296-5301.

4. H. M. El-Kaderi, J. R. Hunt, J. L. Mendoza-Cortés, A. P. Côté, R. E. Taylor, M. O'Keeffe, O. M. Yaghi, *Science* **2007**, *316*, 268-272.

5. J. R. Hunt, C. J. Doonan, J. D. LeVangie, A. P. Côté, and O. M. Yaghi, *J. Am. Chem. Soc.* **2008**, *130*, 11872-11873.

6. W. Niu, M. D. Smith, J. J. Lavigne, *J. Am. Chem. Soc.* **2006**, *128*, 16466-16467.

7. W. Niu, C. O'Sullivan, B. M. Rambo, M. D. Smith, J. J. Lavigne, *Chem. common.* **2005**, 4342-4344.

7. R. W. Tilford, W. R. Gemmill, H. C. zur Loye, J. J. Lavigne, *Chem. Mater*. **2006**, *18*, 5296-5301.

8. R. W. Tilford, W. R. Gemmill, H. C. zur Loye, J. J. Lavigne, *Chem. Mater*. **2006**, *18*, 5296-5301.

9. R. W. Tilford, S. J. Mugavero III, P. J. Pellechia, J. J. Lavigne, *Adv. Mater.* **2008**, *20*, 2741-2746.

10. Y. Li, J. Ding, M. Day, Y. Tao, J. Lu, M. DLiorio, *Chem. Mater.***2003**, *15*,4936-4943.

11. P. Kuhn, M. Antonietti, A. Thomas, *Angew. Chem. Int. Ed.* **2008**, *47*, 3450-3453.

12. J. Weber, A. Thomas, *J. Am. Chem. Soc.* **2008**, *130*, 13333-13337.

13. E. R. Cooper, C. D. Andrews, P. S. Wheatley, P. B. Webb, P. Wormald, R. E. Morris, *Nature* **2004**, *430*, 1012-1016.

14. D. M. Rudkevich, *Eur. J. Org. Chem.* **2007**, 3255-3270.

15. S. S. Han, H. Furukawa, O. M. Yaghi, W. A. Goddard III, *J. Am. Chem. Soc.*, **2008**, *130*, 11580-11581.

16. Y. Li and R. T. Yang, *AIChE Journal*, **2008**, *54*, 269-279.

Chapter 2

A Belt-Shaped, Blue Luminescent, and Semiconducting Covalent Organic Framework

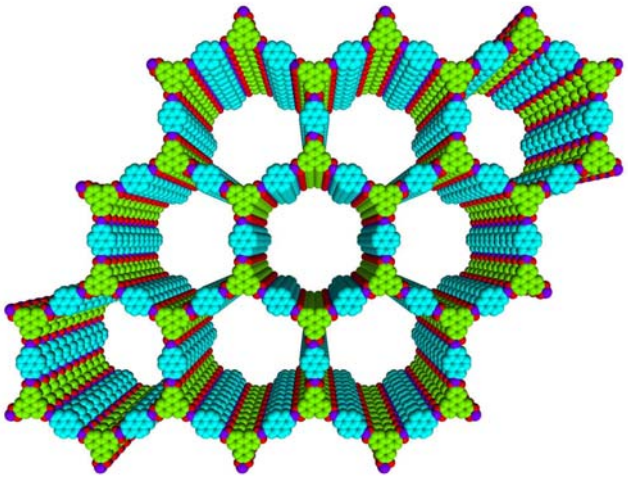

2-1. Abstract

In this part, the author reports the first example of a luminescent and semiconducting COF (TP-COF), which adopts a belt shape and consists of pyrene and triphenylene functionalities alternatively linked in a mesoporous hexagonal skeleton (Fig. 2-1, TP-COF).

A new family of covalent organic framework based on π electron system was synthesized by condensation polymerization with triphenylene and pyrene derivatives as monomers (TP-COF). TP-COF adopts belt morphology with thickness of about 100 nm, width of about 300 nm, and length of micrometers. When triphenylene and pyrene units were selectively excited by ultraviolet and visible lights, TP-COF displays strong blue fluorescence at 474 nm, as a result of an efficient energy transfer between two units. This result demonstrates that TP-COF collects photons of a wide range covering from ultraviolet to the visible regions and converts them to blue emission efficiently. In addition, due to the ultimate π stacking of large π-conjugated components, TP-COF is electrically semiconducting. The electric current can be repetitively on/off switched without any deterioration. Upon doping with iodine, the electric current was increased remarkably, which suggests that TP-COF is *p*-type semiconductor.

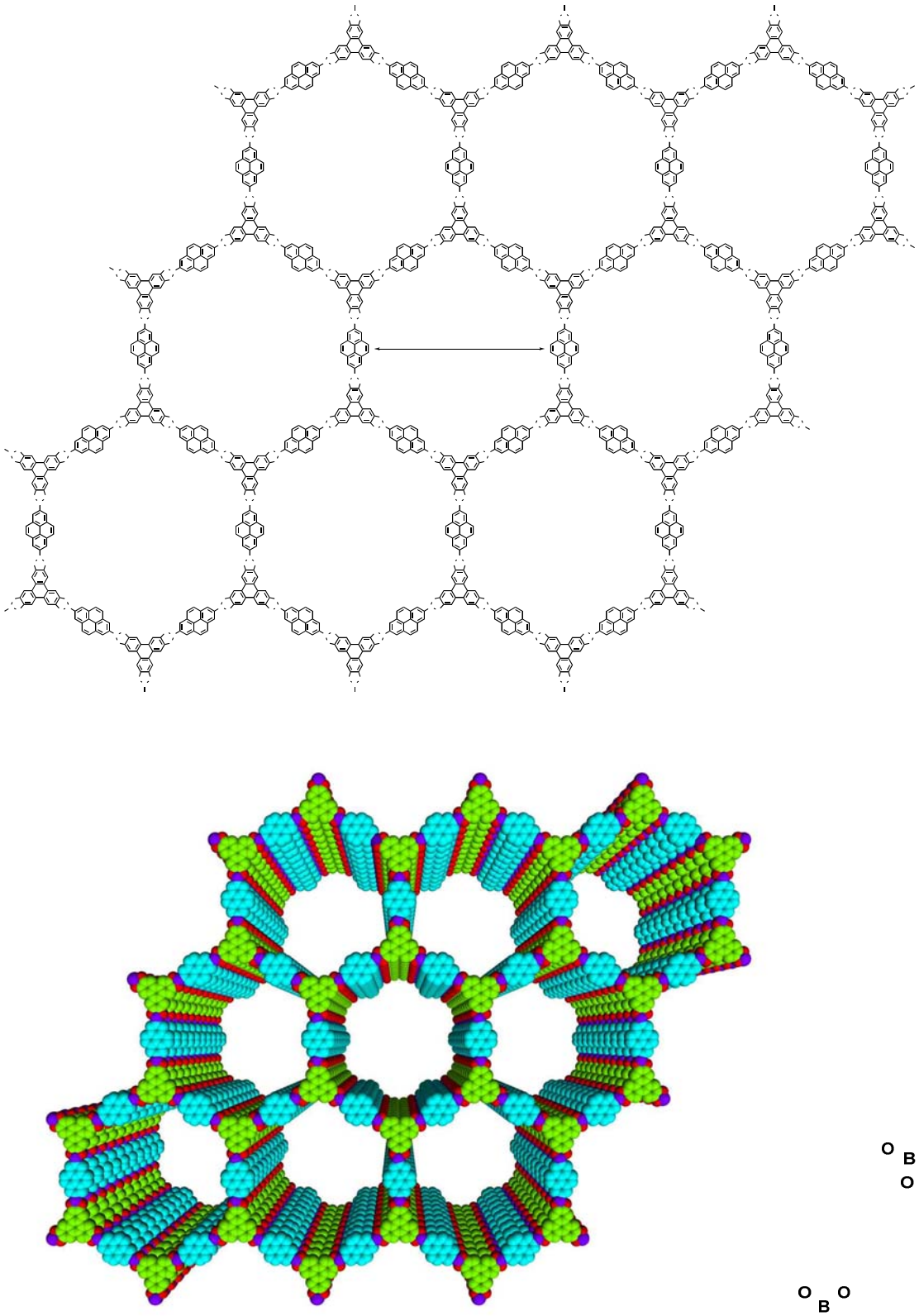

Figure 2-1. Schematic representation of TP-COF.

2-2. Design of TP-COF

As shown in Figure 2-1, TP-COF was topologically designed by employing a D_{3h} symmetric monomer as corner and a D_{2h} symmetric monomer as edge for pore hexagons and synthesized by a condensation reaction of 2,3,6,7,10,11-hexahydroxytriphenylene (HHTP) and pyrene-2,7-diboronic acid (PDBA).

2-3. Synthesis and Characterization of TP-COF

Synthesis of TP-COF

In a typical experiment, HHTP (74.58 mg, 0.23mmol) and PDBA (100 mg, 0.345mmol) were mixed in 1,4-dioxane/mesitylene(10mL/10mL) and stirred at 85 °C under Argon for 3 days[1]. The precipitate was collected by centrifugation, washed with anhydrous acetone, and dried at 150 °C under vacuum to give TP-COF (123 mg) as a pale yellow powder in 90% yield.

FT IR Spectral Profiles

FT IR spectroscopy shows that vibrational bands due to boronate ester ring appeared at 1345, 1328, 1246 and 1049 cm^{-1}, whereas the hydroxyl bands of the starting materials were strongly attenuated in TP-COF, indicating the condensation of two monomers (Fig. 2-2, Table 2-1).

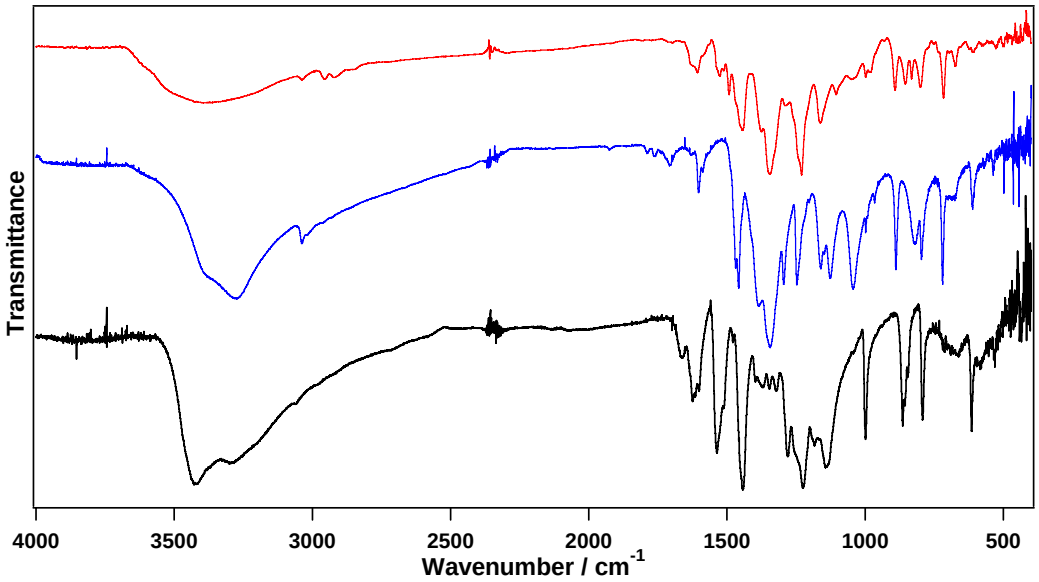

Figure 2-2.FT IR spectra of PDBA, HHTP and TP-COF. The red, blue and black curves are IR spectra of TP-COF, PDBA and HHTP, respectively.

Peak (cm^{-1})	**Assignment and Notes**
3395.07 (m)	O–H stretch from the end $B(OH)_2$ or OH groups
3037.34 (w)	Aromatic C–H stretch from pyrene units
2955.38 (w)	C–H stretching from triphenylene building blocks
2922.11 (w)	
2871.01 (w)	
1630.3 (w)	C=C stretch for fused aromatics. Also observed in HHTP
1525.9 (m)	C=C vibrational mode of phenyl ring. Characteristic band
1492.63 (m)	C=C vibrational modes for triphenylene building blocks, Characteristic bands for triphenylene
1443.94 (m)	
1344.62 (s)	B–O stretch, characteristic band for boroxoles
1328.23 (s)	B–O stretch

1245.79 (s)	C–O stretch, characteristic for boroxoles
1163.8 (m)	C–H in-plane bending modes
1105.98 (m)	
1049.09 (m)	B–C stretch
855.28 (m)	C–H out-of-plane bending modes for *p*-substituted aromatic rings
832.62 (m)	
800.80 (m)	C–H out-of-plane bending modes
716.91 (m)	
675.45 (m)	
609.88 (w)	

Table 2-1:Peak assignments for FT-IR spectrum of TP-COF.

FE SEM of TP-COF

FE SEM images of TP-COF reveal that the condensation polymerization of PDBA and HHTP afford belts with length extended to micrometers and width of about 300 nm and thickness of 100 nm (Fig. 2-3). A close examination shows no other morphologies are observable (Fig. 2-4).

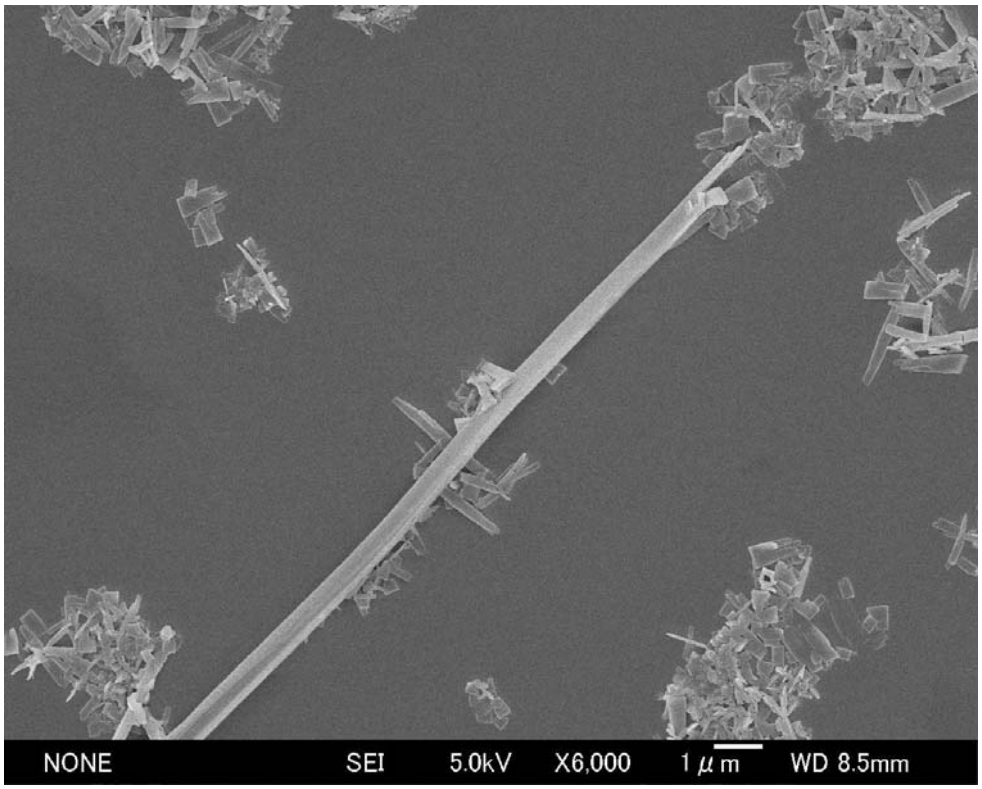

Figure 2-3.FE SEM of TP-COF.

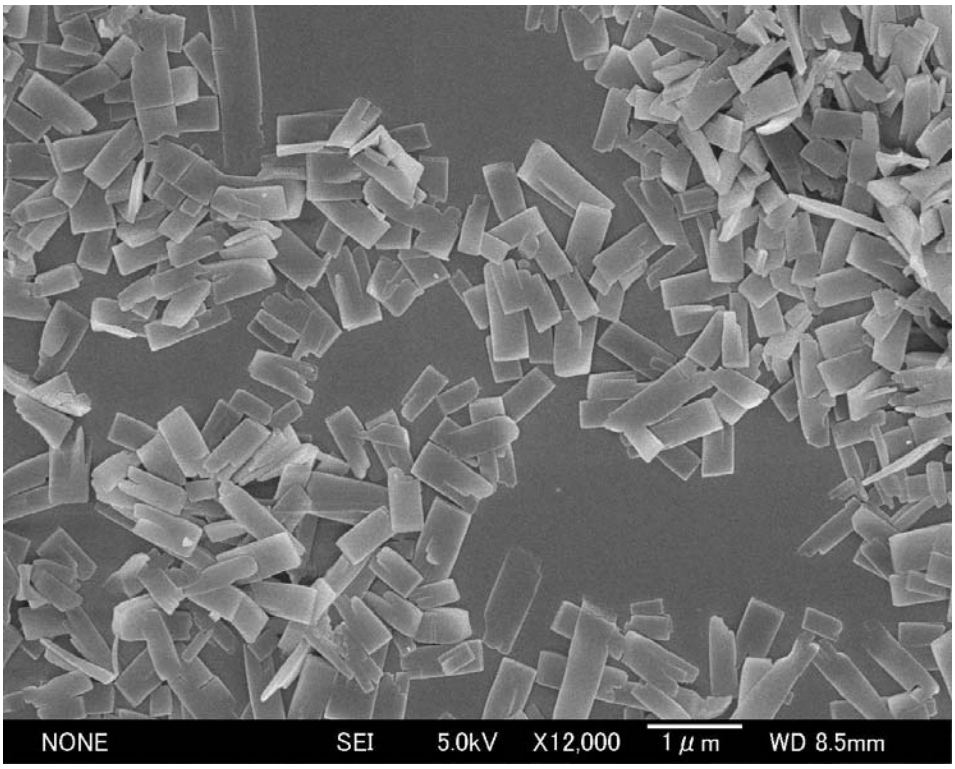

Figure 2-4.FE SEM of TP-COF.

HR TEM of TP-COF

To further investigate the structure, high resolution TEM was performed. As shown in Figure 2-5, clear aligned patterns were observed along the (110) facet. From the aligned layer structure, the distance between sheets is estimated to be 3.40 Å, which is reasonable for π-π stacking. Such a belt texture with a uniform morphology and the direct visualization of a stacked sheet structure are unprecedented for COFs. To our surprise, along the (001) facet, hexagonal mesostructure can be observed and enables the estimation of center-to-center distance between the neighbouring pores to be about 3.3 nm (Fig. 2-6).

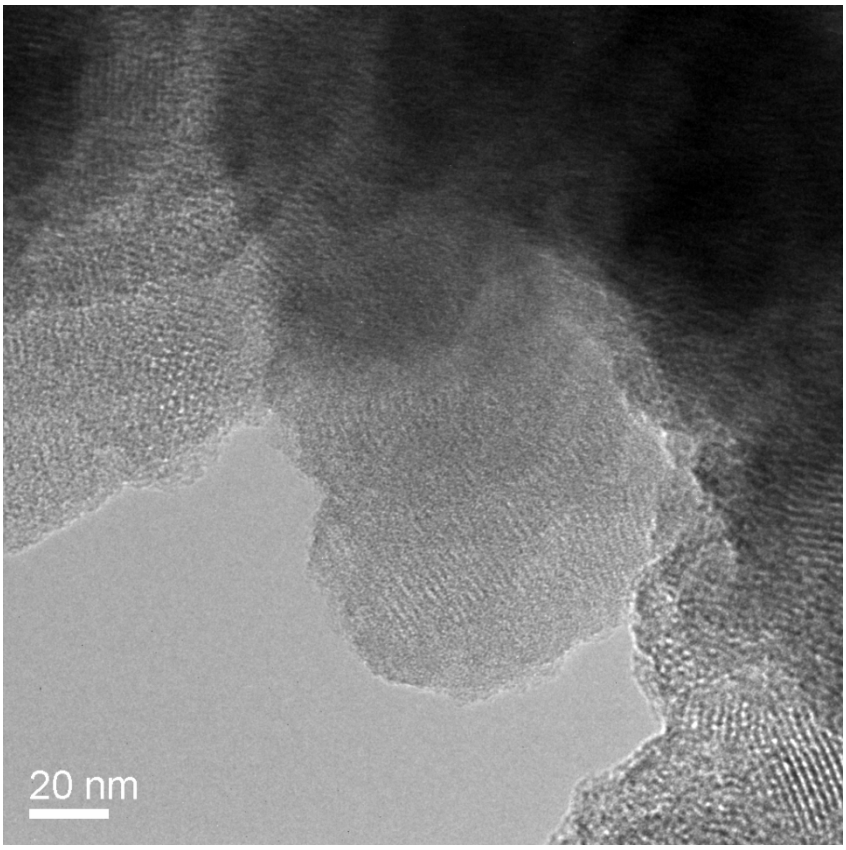

Figure 2-5.HR TEM of TP-COF.

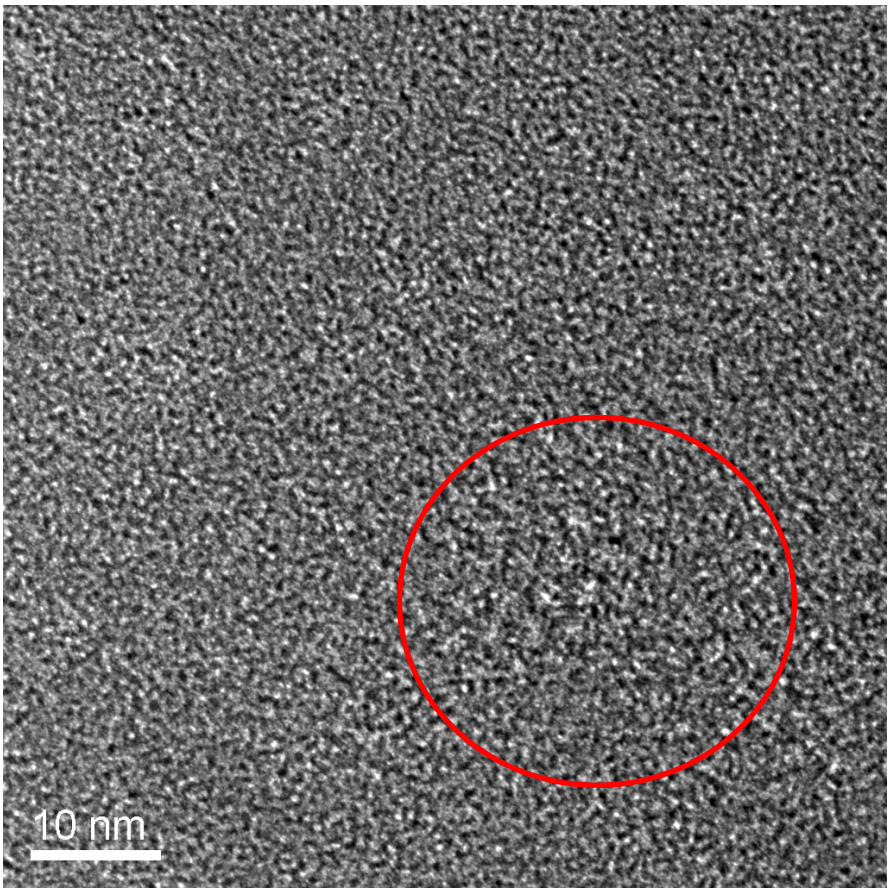

Figure 2-6.HR TEM of TP-COF.

Experimental PXRD Pattern

Powder x-ray diffraction (PXRD) exhibits a main diffraction peak due to 100 at 2.70°, along with diffractions owing to 110, 200, 210, 300, 310, and 001 at 4.74°, 5.46°, 7.26°, 8.24°, 9.54° and 26.32°, respectively (Fig. 2-7, red curve).

Simulation of PXRD Pattern and Crystal Packing

To elucidate the lattice packing, we first carried out semi-empirical calculation at PM3 level to optimize the geometry of the whole pore unit structure and further optimized the molecular geometry of the repeating unit in the single unit cell at

B3LYP/6-31G(d) by using Gaussian 03 program[2]. Final lattice parameters were determined after performing Pawley refinement by using Reflex, a software package for crystal structure determination from the PXRD pattern, implemented in MS modelling (ver4.2)[3]. Simulation using the space group of *P*6/mmm (No. 191) with $a = b = 37.5412$ Å and $c = 3.3784$ Å gives a PXRD pattern in good agreement with the experimentally observed one (Fig. 2-7). All the diffraction peaks can be reasonably assigned. On the other hand, a staggered model using the space group of *P*63/mmc (No. 194) does not reproduce the experimental PXRD pattern (Fig. 2-8). Therefore, the 2-D sheets crystallize in an eclipsed fashion to give a perfect superimposition of the triphenylene and pyrene units on themselves (Fig. 2-1, Fig. 2-7). Such a crystalline structure would provide open and aligned mesopores of 3.26 nm in diameter (Fig. 2-7).

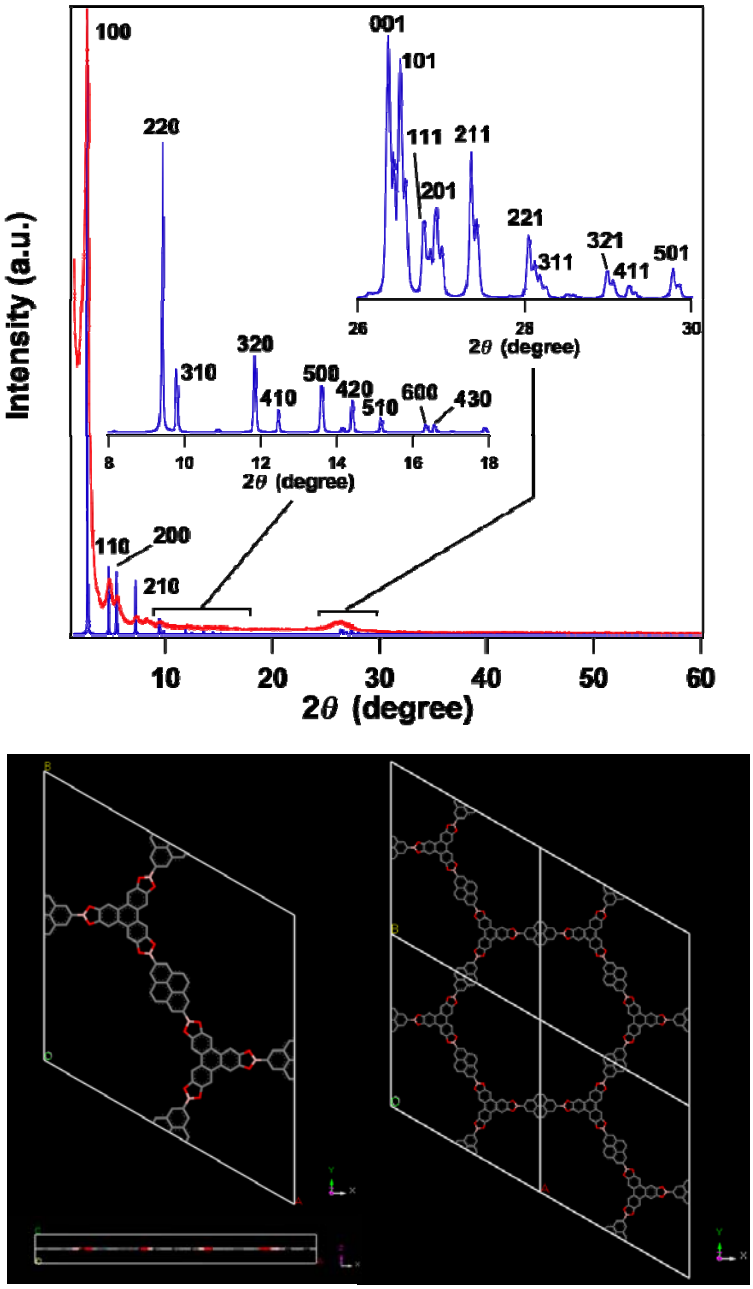

Figure 2-7.PXRD pattern of TP-COF and simulation of crystal lattice packing in the eclipsed form. In the upper figure, the red curve represents the experimental PXRD pattern and the blue pattern is calculated from the eclipsed crystal packing (Crystal space group *P*6/mmm; No. 191). The calculated pattern simulates the experimental data well. The insets show the assignment of PXRD signals. The lower figure shows the eclipsed crystal lattice packing of TP-COF. The pore size is 3.26 nm in diameter in the defined structure.

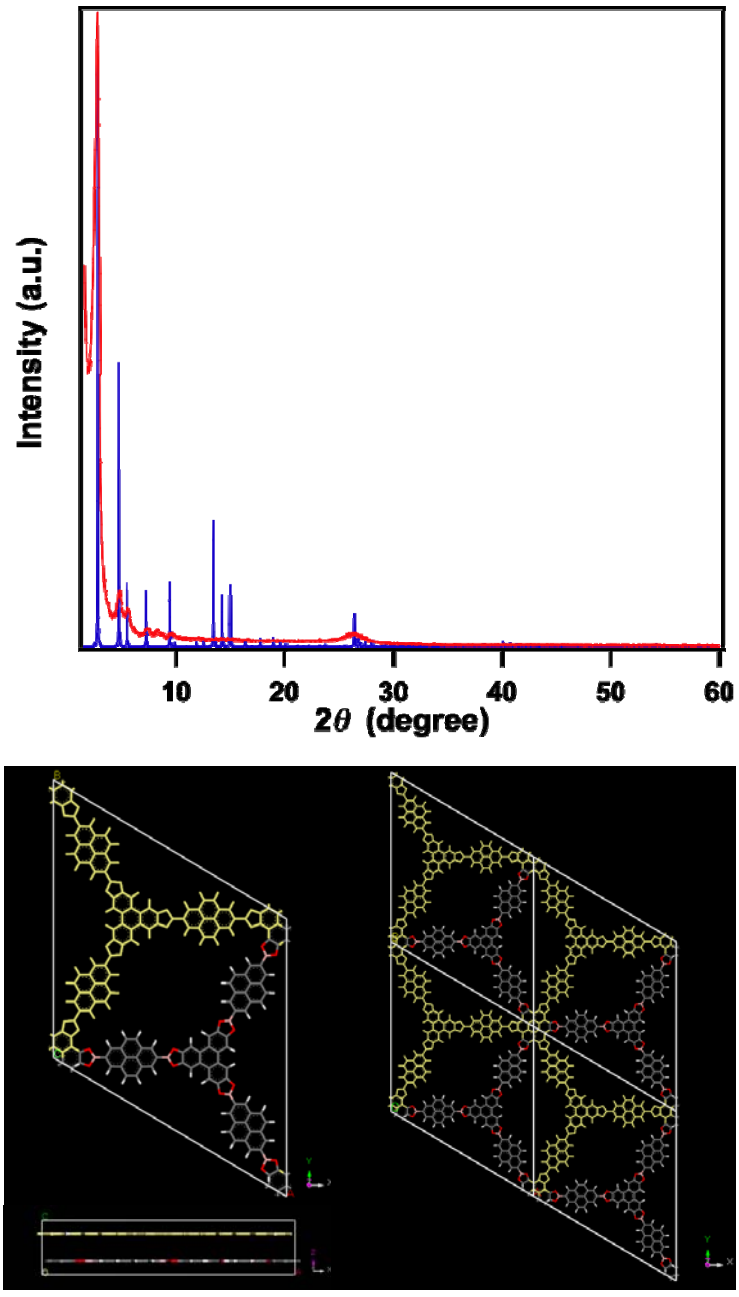

Figure 2-8.PXRD pattern of TP-COF and simulation of crystal lattice packing in the staggered form. In the upper figure, the red curve represents the experimental PXRD pattern and the blue pattern is calculated from the staggered crystal packing (Crystal space group *P*63/mmc; No. 194). The simulated pattern does not fit the experimental data at all. The lower figure shows the staggered crystal lattice packing. In this case, the pore is covered and the pore size is significantly smaller than the experimental one.

Formula	$C_{84}O_{12}B_6$
Formula weight	1265.78
Crystal system	Hexagonal
Space group	*P*6/mmm (No.191)
Unit cell dimensions	$a = b = 37.5412$ Å $c = 3.3784$ Å
Cell volume	4123.42 $Å^3$
Density calculated	0.510 g/cm^3

Table 2-2: Refined crystal data

Atom	Wyck.	x	y	z
C1	12*q*	0.29457	0.62814	0.50000
C2	12*q*	0.33388	0.59643	0.50000
C3	12*q*	0.37097	0.59167	0.50000
O4	12*q*	0.37899	0.55964	0.50000
C7	12*q*	0.42428	0.51126	0.50000
C8	12*q*	0.44513	0.48902	0.50000
C10	12*q*	0.42390	0.44477	0.50000
B5	6*m*	0.42181	0.57819	0.50000
C6	6*m*	0.44552	0.55448	0.50000
C9	6*m*	0.48905	0.51095	0.50000

Table 2-3: Fractional atomic coordinate

Nitrogen Sorption Isotherm Measurement

We carried out nitrogen sorption isotherm measurement to investigate the porosity of TP-COF. As shown in Figure 2-9a, TP-COF exhibits a typical type IV nitrogen sorption curve, indicative of a mesoporous character[4]. BET calculation gives specific surface area and pore volume of 868 m^2 g^{-1} and 0.7907 cm^3 g^{-1}, respectively. Estimation of pore size with the DFT model shows a diameter of 3.14 nm (Fig. 2-9b), which is close to the theoretical one. Pore distribution profile exhibits that in TP-COF the specific surface area originates predominately from the persistent mesopores, whereas contribution of other pores formed between belts or from defects are small (Fig. 2-9b). All the above results indicate that TP-COF is a crystalline material with a uniformly sized mesopore formed via the eclipsed packing of the polymeric sheets.

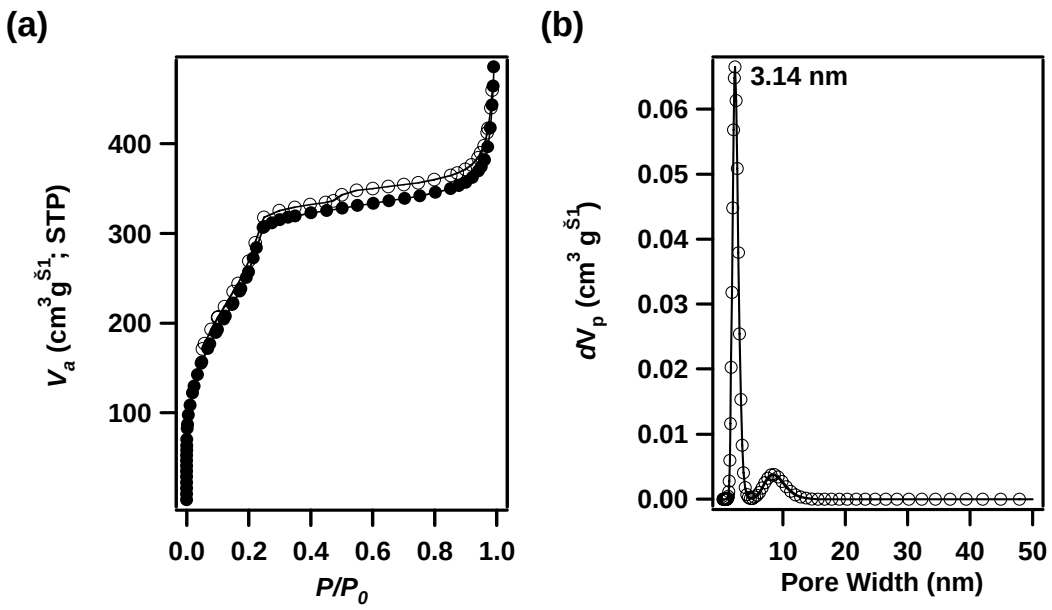

Figure 2-9.(a) Nitrogen adsorption (●) and desorption (○) isotherm profiles of TP-COF at 77 K. (b) Pore size distribution of TP-COF by DFT modeling on the N_2 adsorption isotherms.

Fluorescence Spectral Profiles

Fluorescence microscopy exhibits that the belts of TP-COF are highly blue luminescent (Fig. 2-10a). Condensed poly(boronate ester)s bearing fluorene units have been reported to be blue-emissive materials[5,6]. Fluorescence spectroscopy shows that TP-COF emitted a luminescence at 474 nm, upon excitation of the pyrene units at 376 or 417 nm (Fig. 2-10b, dotted curve). On the other hand, when a solid sample of HHTP monomer was excited at 340 nm, it emitted fluorescence at 402 nm with a shoulder at 424 nm. Since this emission is partially overlapped with the absorption band of the pyrene, the triphenylene units in TP-COF have a chance to communicate photochemically with the pyrene moieties by energy transfer from the excited state. Excitation of the triphenylene units in TP-COF at 340 nm resulted in negligibly weak emission at 402 nm from the triphenylene units but a strong emission from the pyrene

moieties at 474 nm (Fig. 2-10b, black curve), where the fluorescence intensity ratio $I_{474\ nm}/I_{402\ nm}$ was as high as 16.

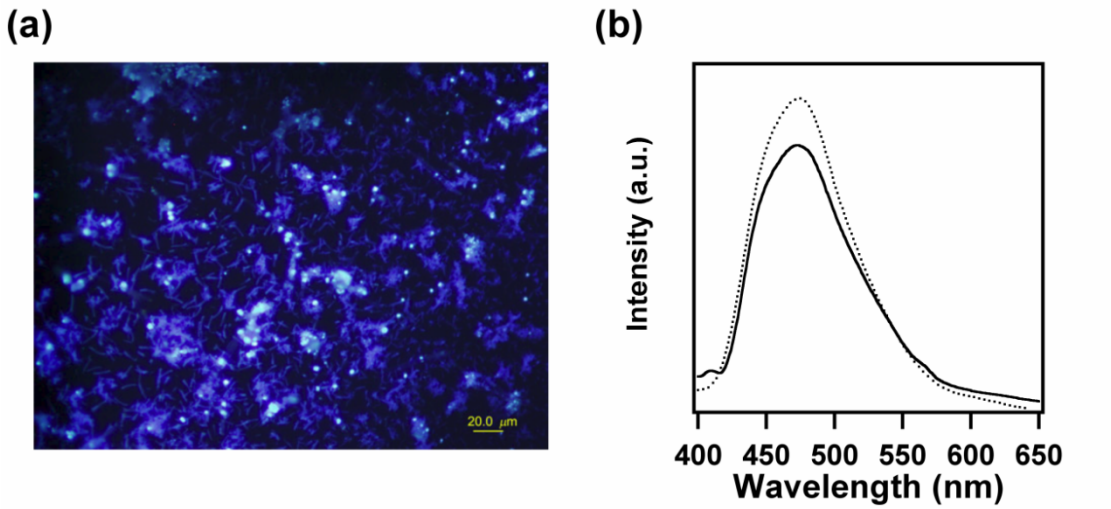

Figure 2-10.(a) Fluorescence image of TP-COF. (b) Fluorescence spectra of TP-COF upon excitation at 340 nm (black curve) and 376 nm (dotted curve) at 25 °C.

In sharp contrast, when a 2:3 solid mixture of HHTP and PDBA was excited at 340 nm, it emitted predominately at 402 nm to furnish a low $I_{474\ nm}/I_{402\ nm}$ ratio (0.6). Therefore, the strong pyrene fluorescence, observed for TP-COF upon 340 nm excitation, is obviously due to an intramolecular singlet energy from the triphenylene units to pyrene units. Comparison of the excitation spectrum with diffuse reflectance UV-Vis spectrum (Kubelka-Munk spectrum; Fig. 2-11), the quantum yield of energy transfer was estimated to be 60%. Therefore, by virtue of the triphenylene units, TP-COF can harvest photons of a wide wavelength range covering from ultraviolet to visible regions and converts them to blue emission.

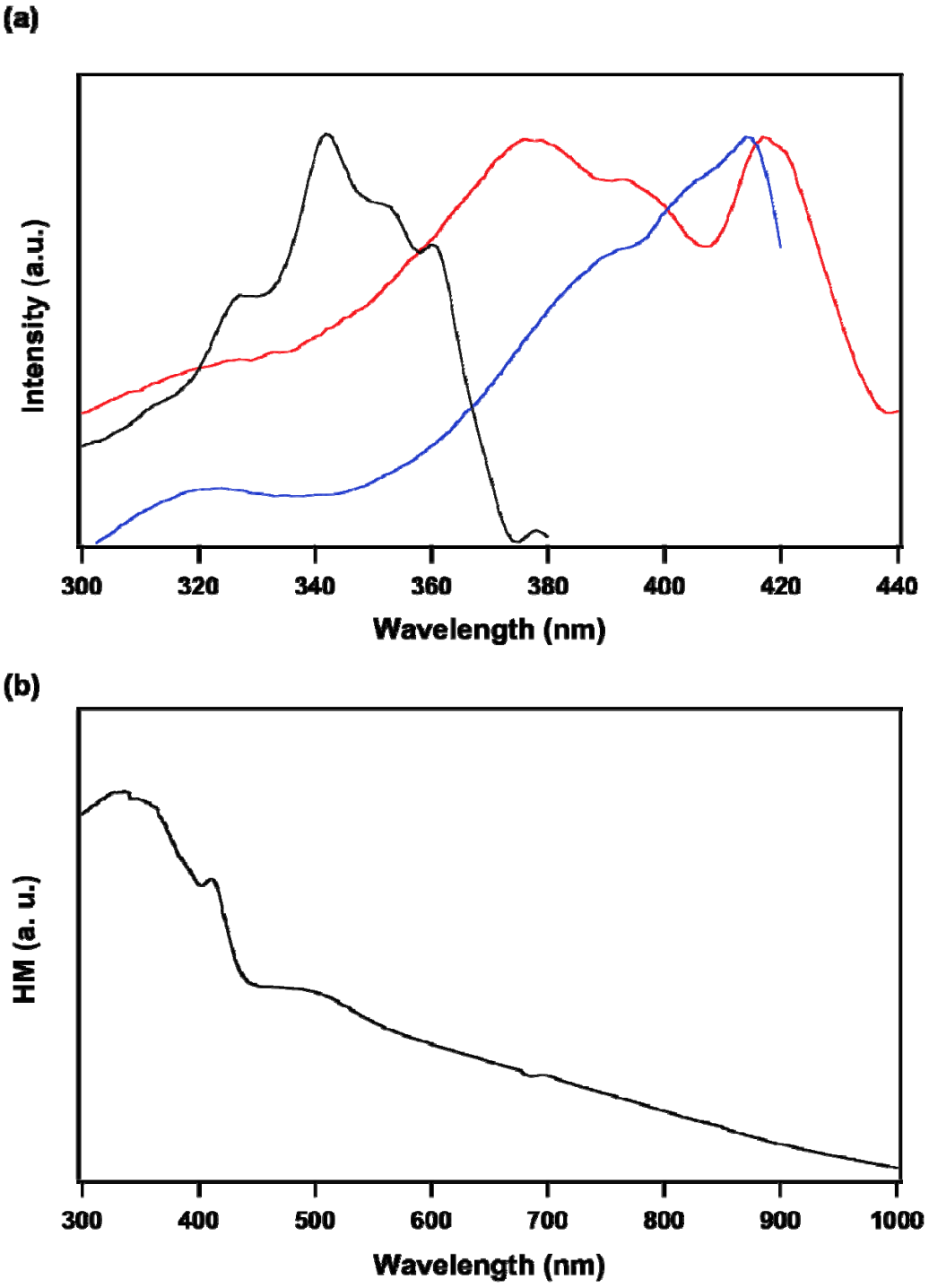

Figure 2-11.(a) Normalized fluorescence excitation spectra of PDBA (blue curve), HHTP (black curve) and TP-COF (red curve). (b) Diffuse reflectance UV-VIS-NIR spectrum of TP-COF.

Fluorescence Anisotropy of TP-COF

Along this line, we further investigated the fluorescence anisotropy of TP-COF upon excitation with a polarized light. When a chromophore with a restricted Brownian motion is excited by a polarized light, it emits a polarized fluorescence. However, the fluorescence should be depolarized when the excitation energy migrates randomly within the lifetime of the excited state. Here, fluorescence anisotropy (p) is defined by $(I_{||} - GI_{\perp})/(I_{||} + GI_{\perp})$, where $I_{||}$ and $I_{\perp}$ are fluorescence intensities of parallel and perpendicular components relative to the polarity of the excitation light, respectively, where G is an instrumental correction factor. The 2:3 solid mixture of HHTP and PDBA shows a p value of 0.058. In sharp contrast, TP-COF under identical conditions exhibited a significantly depolarized fluorescence with an extremely low p value of 0.017. This observation reveals that TP-COF not only mediates energy transfer between components but facilitates energy migration over the crystalline belt as well.

Semiconducting Property of TP-COF

Single crystals of pyrene and triphenylene have been reported to function as semiconductor[7,8]. Due to the ultimate π-stacking of these large π-conjugated components, TP-COF may have a high probability of becoming electrically semiconductive. We investigated this possibility by measuring the electric conductivity with a 10-μm width Pt gap using a two-probe method. TP-COF in air at 25 °C shows an almost linear I-V profile (Fig. 2-12a, blue curve), while the gap itself is silent

irrespective of voltage bias (black curve). For example, at 2-V bias voltage, the electric current is 4.3 nA (Fig. 2-12b). In contrast, a 2:3 mixture of HHTP and PDBA shows a low current (79 pA) under otherwise identical conditions. Moreover, the electric current can be on/off switched repeatedly for many times without significant deterioration (Fig. 2-12b). The relatively high electric current observed for TP-COF is likely related to the highly order structure that enables the formation of a conductive path. Upon doping with iodine, the electric current was increased (Fig. 2-12a, red curve), suggesting a *p*-type semiconductor character of TP-COF.

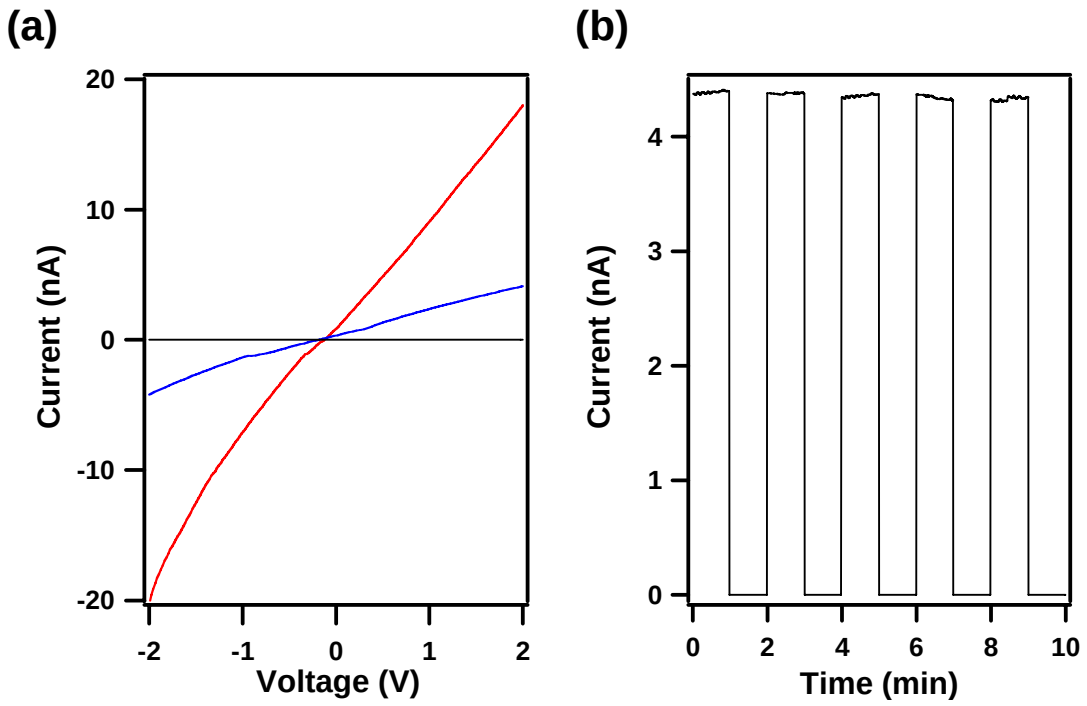

Figure 2-12.(a) I-V profile of TP-COF between a 10-μm width Pt gap (black curve: without TP-COF; blue curve: with TP-COF; red curve: with iodine-doped TP-COF). (b) Electric current when 2-V bias voltage is turned on or off.

2-4. Conclusion

Exploration of functional COFs is a subject with a high probability to the development of new materials. In summary, the author demonstrated the synthesis of a new COF based on the condensation reaction of triphenylene and pyrene monomers. TP-COF is highly luminescent, harvests a wide wavelength range of photons and allows energy transfer and migration. Furthermore, TP-COF is electrically conductive and capable of repetitive on-off current switching at room temperature. These characters are unique and clearly originate from the highly ordered structure of TP-COF. By filling the mesopores with photoactive molecules such as electron acceptor, it will lead to the fabrication of COF-based optoelectronic device, which is one of the targets worthy of further investigation.

2-5. Experimental Section

Materials

THF was distilled over benzophenoneketyl under argon before use. Cyclohexane was distilled under argon before use. Pyrene, bispinacolatodiboron, anhydrous 1,4-dioxane (99.8%) and anhydrous acetone (99.8%) were purchased from Wako Chemicals. 2,3,6,7,10,11- hexahydroxytriphenylene (HHTP) and mesitylene (98%) were purchased from TCI. 4,4'-Di-*tert*-butyl-2,2'-bipyridine was purchased from Aldrich. Sodium periodate and hydrochloric acid were purchased from Kanto Co. Ltd. Methoxy(cyclooctadiene)iridium(I) dimer was purchased from Alfa Aesar Chemicals.

Silica gel Wakogel C–300HG was used for column chromatography. Deuterated solvents for NMR measurements were obtained from Cambridge Isotope Laboratories, Inc. Pyrene-2,7-diboronic ester was prepared according to reported methods[9] (Scheme. 2-1).

Synthesis

All reactions were performed under argon using Schlenk line technique.

PDBA: A THF/water mixture (60 mL, 4/1 in vol.) of pyrene-2,7-diboronic ester (1g, 2.21 mmol) and sodium periodate (2.84 g, 13.25 mmol) was stirred for 30 min and was added with aqueous hydrochloric acid (1N, 3.1 ml, 3.1 mmol). The reaction mixture was stirred at room temperature overnight, diluted with water (30 ml) and extracted with ethyl acetate (3 × 50 ml). The combined extracts were washed with water (3 × 30 ml) and brine (30 ml), dried over sodium sulfate, filtered, and concentrated to dryness. The solid residue after rinsed with small portions of hexane gave **PDBA** as brown solid in 98% yield (638 mg)[10].

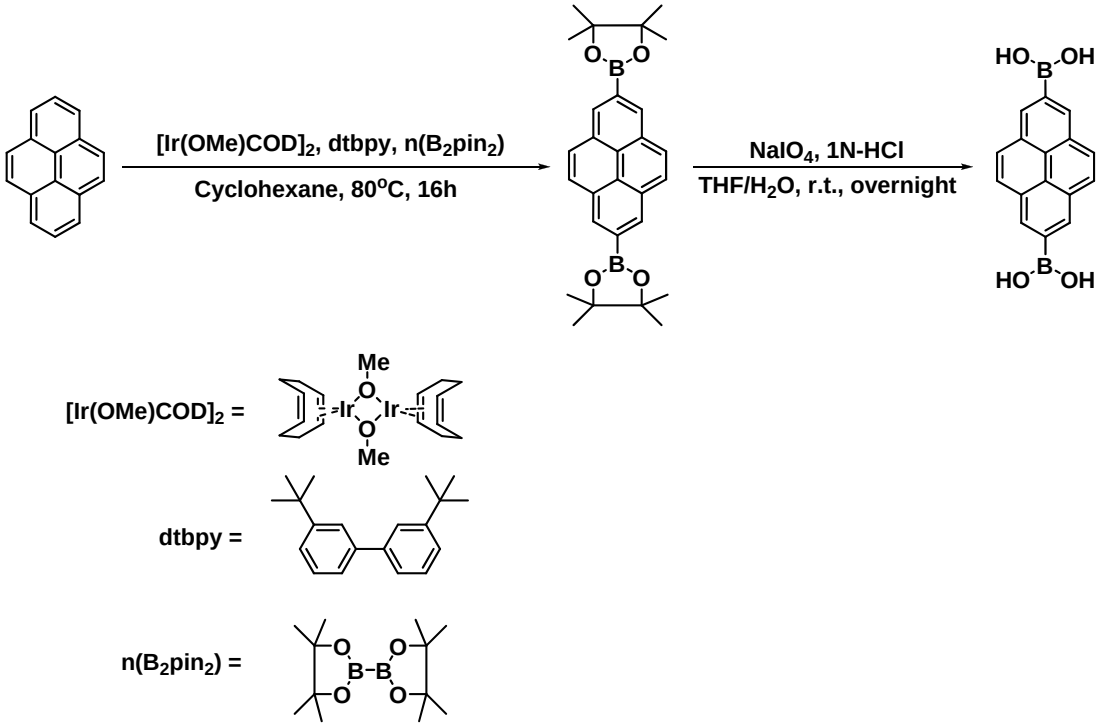

Scheme.2-1. Syntheses of Pyrene-2,7-diboronic ester and PDBA.

^{1}H NMR (400 MHz, DMSO-d^{6}): δ ppm 8.68 (4H, s, 1,3,6,7-*H*-pyrene), 8.44 (4H, s, 4,5,9,10-*H*-pyrene), 8.16 (4H, s, BO–*H*)(Shown in Fig. 2-13a).

^{13}C NMR (100 MHz, DMSO-d^{6}): δ ppm 130.80, 130.03, 127.44, 124.95.

MALDI–TOF MS for $C_{16}H_{12}B_2O_4$ (Cacld.290.0922), m/z = 290.2092 ($[M + H]^+$) (Shown in Fig. 2-13b).

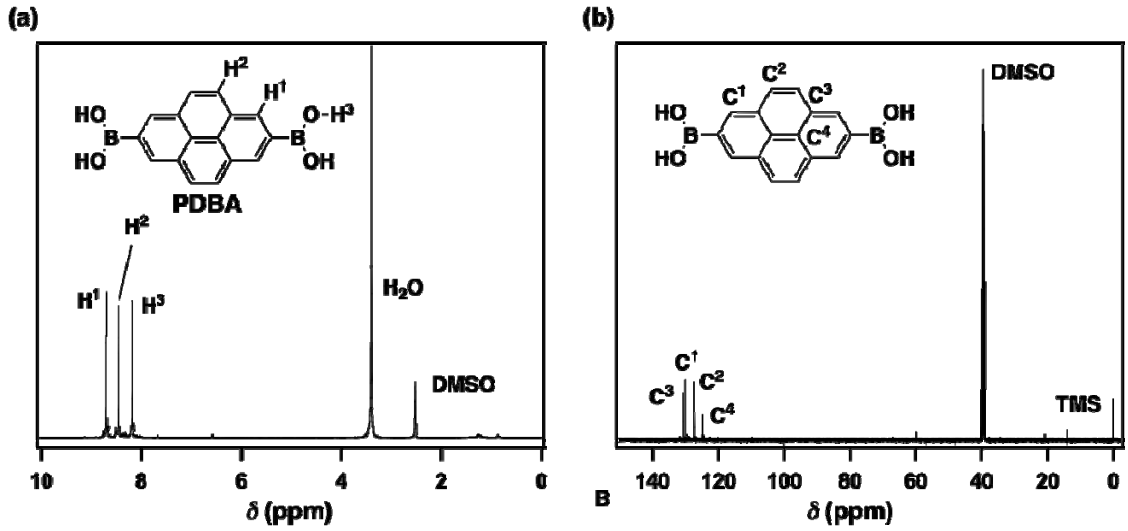

Figure 2-13.(a) ^{1}H and (b) ^{13}C NMR spectra of PDBA in DMSO-d^{6}.

TP-COF: A 1,4-dioxane/mesitylene mixture (20 mL, 1/1 in vol.) of PDBA (100 mg, 0.345 mmol) and HHTP (74.58 mg, 0.23 mmol) was stirred at 85 °C for 3 days under argon. The precipitate was collected by centrifugation, washed with anhydrous acetone and dried at 150 °C under vacuum to give TP-COF (123 mg) as a pale yellow powder in 90% yield.

Measurements

^{1}H and ^{13}C NMR spectra were recorded on JEOL models JNM–LA400 or JNM–LA500 NMR spectrometers, where chemical shifts (δ in ppm) were determined with a residual proton of the solvent as standard. Infrared (IR) spectra were recorded on a JASCO model FT IR–6100 Fourier transform infrared spectrometer. UV-Vis-IR diffuse reflectance spectrum (Kubelka-Munk spectrum) was recorded on a JASCO model V-670 spectrometer equipped with integration sphere model IJN-727. Matrix–assisted laser desorption ionizationtime–of–flight mass (MALDI–TOF–MS)

spectra were recorded on an Applied Biosystems BioSpectrometry model Voyager–DE–STR spectrometer in reflector or linear mode using 9–nitroanthracene or dithranol as matrix. Field emissionscanning electron microscopy (FE SEM) was performed on a JEOL model JSM–6700 FE–SEM operating at an accelerating voltage of 1.5 or 5.0 kV. The sample was prepared by drop–casting an acetone suspension onto mica substrate and then coated with gold. Transmission Electron Microscope (TEM) images were obtained on a JEOL model JEM–3200 microscope. The sample was prepared by drop–casting an acetone suspension of TP-COF onto a copper grid. Powder X–ray diffraction (PXRD) data were recorded on a Rigaku model RINT Ultima III diffractometer by depositing powder on glass substrate, from $2\theta = 1.5°$ up to 60° with 0.02° increment at 25°C.

Nitrogen sorption isotherms were measured at 77 K with a Bel Japan Inc. model BELSORP-mini II analyzer. Before measurement, the samples were degassed in vacuum at 200 °C for more than 6h. The Brunauer-Emmett-Teller (BET) method was utilized to calculate the specific surface areas. By using density functional theory (DFT) model, the pore volume was derived from the sorption curve.

Electrical measurements were carried out at 25 °C in air on TP-COF or I_2-doped TP-COF between 10-μm width Pt electrodes by a two-probe method using a Keithley model 2635 sourcemeter. TP-COF was homogenously dispersed in acetone and casted onto the electrode to give a film. For I_2 doping, the TP-COF electrode was put into an I_2 atmosphere for 1h before measurement.

2-6. References

1. A. P.Côté, H. M. El-Kaderi, H. Furukawa, J. R. Hunt, O. M. Yaghi, *J. Am. Chem. Soc.*,**2007**, *129*, 12914-12915.
2. Gaussian 03, Revision C.02, Frisch, M. J.; Trucks, G. W.; Schlegel, H. B.; Scuseria, G. E.; Robb, M. A.; Cheeseman, J. R.; Montgomery, Jr., J. A.; Vreven, T.; Kudin, K. N.; Burant, J. C.; Millam, J. M.; Iyengar, S. S.; Tomasi, J.; Barone, V.; Mennucci, B.; Cossi, M.; Scalmani, G.; Rega, N.; Petersson, G. A.; Nakatsuji, H.; Hada, M.; Ehara, M.; Toyota, K.; Fukuda, R.; Hasegawa, J.; Ishida, M.; Nakajima, T.; Honda, Y.; Kitao, O.; Nakai, H.; Klene, M.; Li, X.; Knox, J. E.; Hratchian, H. P.; Cross, J. B.; Bakken, V.; Adamo, C.; Jaramillo, J.; Gomperts, R.; Stratmann, R. E.; Yazyev, O.; Austin, A. J.; Cammi, R.; Pomelli, C.; Ochterski, J. W.; Ayala, P. Y.; Morokuma, K.; Voth, G. A.; Salvador, P.; Dannenberg, J. J.; Zakrzewski, V. G.; Dapprich, S.; Daniels, A. D.; Strain, M. C.; Farkas, O.; Malick, D. K.; Rabuck, A. D.; Raghavachari, K.; Foresman, J. B.; Ortiz, J. V.; Cui, Q.; Baboul, A. G.; Clifford, S.; Cioslowski, J.; Stefanov, B. B.; Liu, G.; Liashenko, A.; Piskorz, P.; Komaromi, I.; Martin, R. L.; Fox, D. J.; Keith, T.; Al-Laham, M. A.; Peng, C. Y.; Nanayakkara, A.; Challacombe, M.; Gill, P. M. W.; Johnson, B.; Chen, W.; Wong, M. W.; Gonzalez, C.; and Pople, J. A.; Gaussian, Inc., Wallingford CT, 2004.
3. Accelrys, Material Studio Release Notes, Release 4.2, Accelrys Software, San Diego 2006.
4. K. M. Sing, D. H. Everett, R. A. W. Haul, L. Moscou, R. A. Pierotti, J. Rouquerol, T. Siemieniewska, *Pure & Appl. Chem.***1985**, *57*, 603-619.

5. W. Niu, M. D. Smith, J. J. Lavigne, *J. Am. Chem. Soc.* **2006**, *128*, 16466-16467.

6. Y. Li, J.Ding, M, Day, Y. Tao, J. Lu, M. D'iorio, *Chem. Mater.* **2003**, *15*, 4936-4943.

7. J. M. Warman, M. P. de Haas, G. Dicker, F. C. Grozema, J. Piris, M. G. Debije, *Chem. Mater.* **2004**, *16*, 4600-4609.

8. J. G. Basurto, Z. Burshtein, *Mol. Cryst. Liq. Cryst.***1975**, *31*, 211-217.

9. D. N. Coventry, A. S. Batsanov, A. E. Goeta, J. A. K. Howard, T. B. Marder and R. N. Perutz, *Chem. Commun*. **2005**, 2172-2174.

10. C. C. Tzschucke, J. M. Murphy and J. F. Hartwig, *Org. Lett.* **2007**, *9*, 761-764.

Chapter 3

A Polypyrene–Based Blue-Luminescent, Semiconducting and Photoconductive Covalent Organic Framework

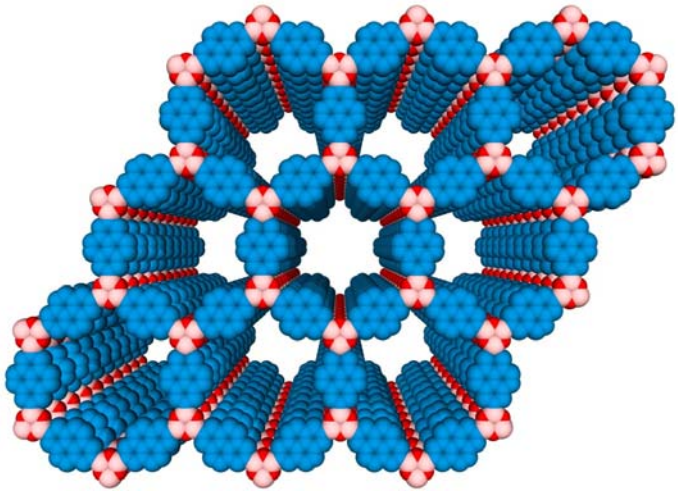

3-1. Abstract

Up to date, among boronic ester based COFs, co-condensation of boronic acid with phenol derivatives has been demonstrated for the synthesis of various boronic ester-based COFs[1–6]. However, self-condensation of boronic acid derivatives has been limited to only one example[1], *i.e.*, benzene 2,7-diboronic acid, which leads to a COF with staggered alignment of 2D polymer sheets.

Herein, the author reports the self-condensation of pyrene diboronic acid to form a new π-electronic COF with polypyrene building blocks (PPy-COF; Fig.3-1). In contrast to the benzene analogue that gives a staggered structure, PPy-COF is unique in that it allows a perfectly eclipsed alignment of 2D polypyrene sheets (Fig. 3-1) to give a micrometer-scale molecular cube. PPy-COF was synthesized by self-condensation polymerization of pyrene diboronic acid (Fig.3-1, PPy-COF). FE SEM shows pure cubic morphology, while HR TEM reveals stacked layers with a separation of about 3.4 Å. Powder X-ray diffraction measurement together with quantum calculation indicates that PPy-COF has a lattice structure with *P*6/mmm space group, where the hexagonal sheets are crystallized in an eclipsed fashion. Nitrogen sorption isotherm measurement shows microporous characters with a pore diameter of 1.88 nm and a large specific area surface. Upon excitation of pyrene units, PPy-COF emits a strong blue luminescence at 484 nm. Significantly depolarized fluorescence anisotropy suggests that the excitation energy is not localized but migrate over the framework. PPy-COF is semiconducting and enables an on/off switch of electric current at room temperature. Moreover, PPy-COF is photoconductive with a quick response to light irradiation and a large

on/off ratio.

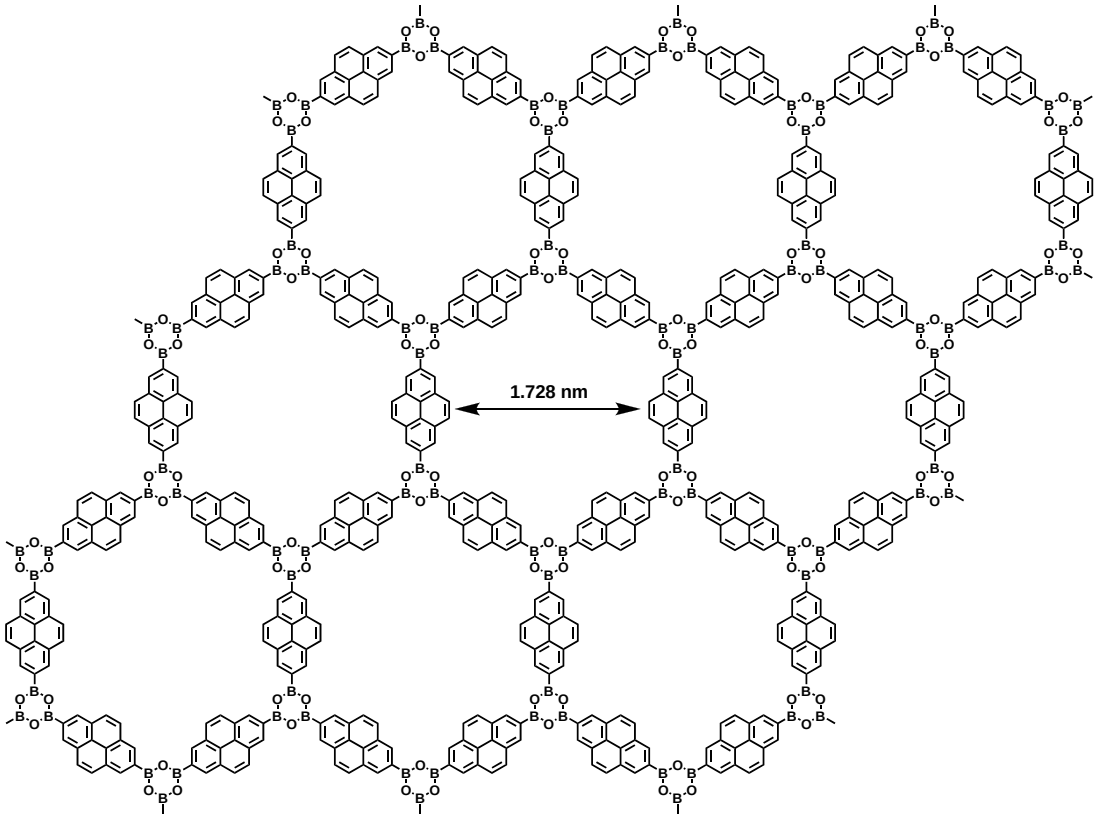

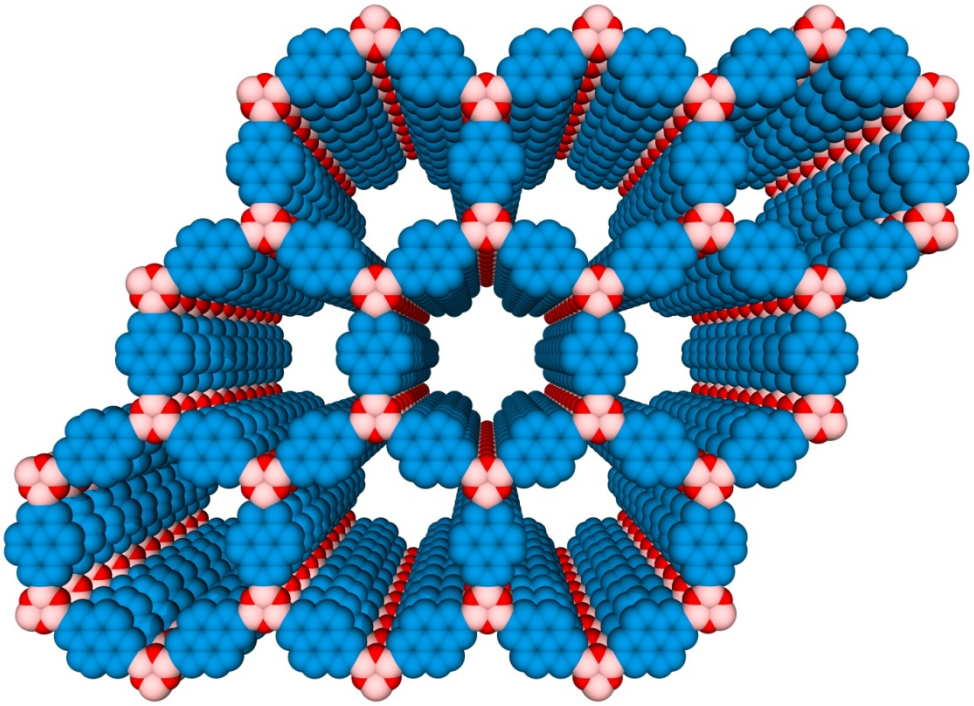

Figure 3-1. Schematic representation of PPy-COF.

3-2. Design of PPy-COF

PPy-COF was designed with a trimerization system of a D_{2h} monomer and synthesized by self-condensation of pyrene 2,7-diboronic acid (PDBA) under solvothermal condition.

3-3. Synthesis and Characterization of PPy-COF

Synthesis of PPy-COF

As a typical example, a 1,4-dioxane/mesitylene(2.5mL/2.5mL) mixture of PDBA (25.0 mg) in a 10-mL pyrex tube was degassed by three freeze-pump-thaw cycles. Then the tube was sealed, kept in autoclave and heated at 120 °C for 2 days. The precipitate was collected by centrifugation, washed with anhydrous acetone, and dried at 150 °C under vacuum, to give PPy-COF (22 mg) in 88% yield as pale yellow solid[3].

FT IR Spectral Profiles

FT IR spectroscopy shows that vibrational bands due to boronate ester ring appeared at 1381, 1339, 1240 and 1048 cm^{-1}, whereas the hydroxyl bands of the starting materials were strongly attenuated in PPy-COF, indicating the self-condensation of PDBA (Fig. 3-2, Table 3-1).

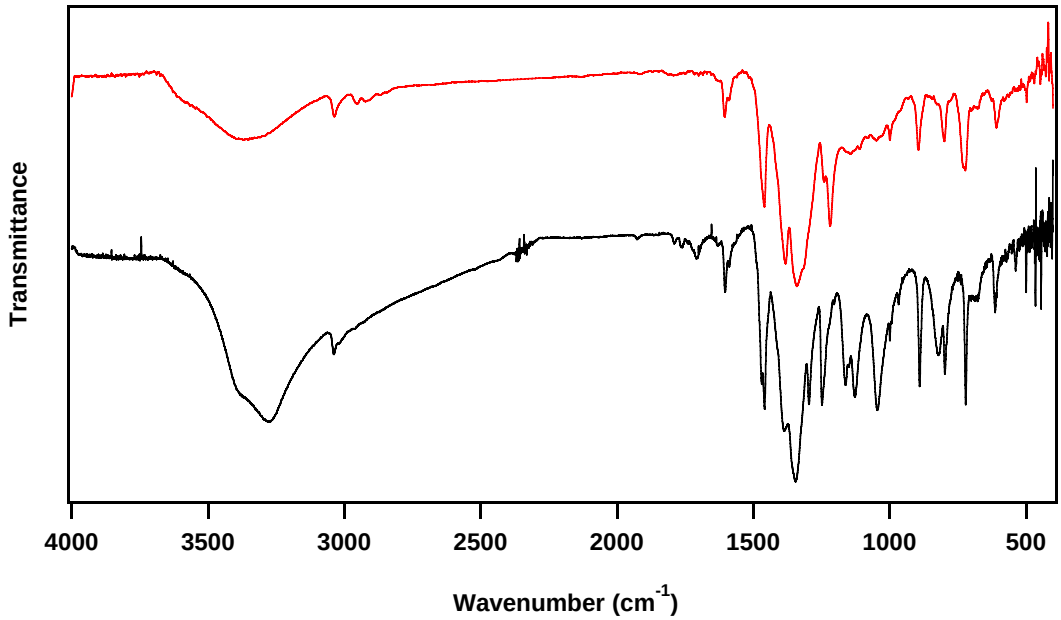

Figure 3-2.FT IR spectra of PDBA (black curve) and PPy-COF (red curve).

Peak (cm^{-1})	**Assignment and Notes**
3369.51 (m)	O–H stretch from the end $B(OH)_2$ or OH groups of PPy-COF.
3036.37 (w)	Aromatic C–H stretch from pyrene unit.
2953.45 (w)	C–H stretching frommesitylene guest molecule.
2922.11 (w)	
2867.15 (w)	
1604.00 (w)	C=C stretch for fused aromatics.
1588.57 (m)	C=C vibrational mode of phenyl ring of pyrene unit.
1458.89 (m)	C=C vibrational modes for p-substituted pyrene unit.
1380.78 (s)	B–O stretch, characteristic band for boroxoles.
1339.32 (s)	B–O stretch, characteristic band for boroxoles.
1316.66 (s)	C–C stretch, characteristic for boroxoles.

1239.52 (m)	C–O stretch, characteristic for boroxoles.
1143.58 (w)	C–H in-plane bending modes.
1109.35 (w)	
1047.64 (m)	B–C stretch.
998.46 (m)	C–H out-of-plane bending modes for *p*-substituted aromatic rings.
893.36 (m)	
798.39 (m)	C–H out-of-plane bending modes
721.73 (m)	
700.03 (w)	
609.88 (w)	

Table 3-1: Peak assignments for FT-IR spectrum of PPy-COF.

FE SEM of PPy-COF

FE SEM shows that PPy-COF assumes cubic shape, while no any other morphologies such as belt, fiber, sphere, or rod are present (Fig.3-3). Close checks at high magnification confirm that the cubes are in micrometer scale with similar dimension.

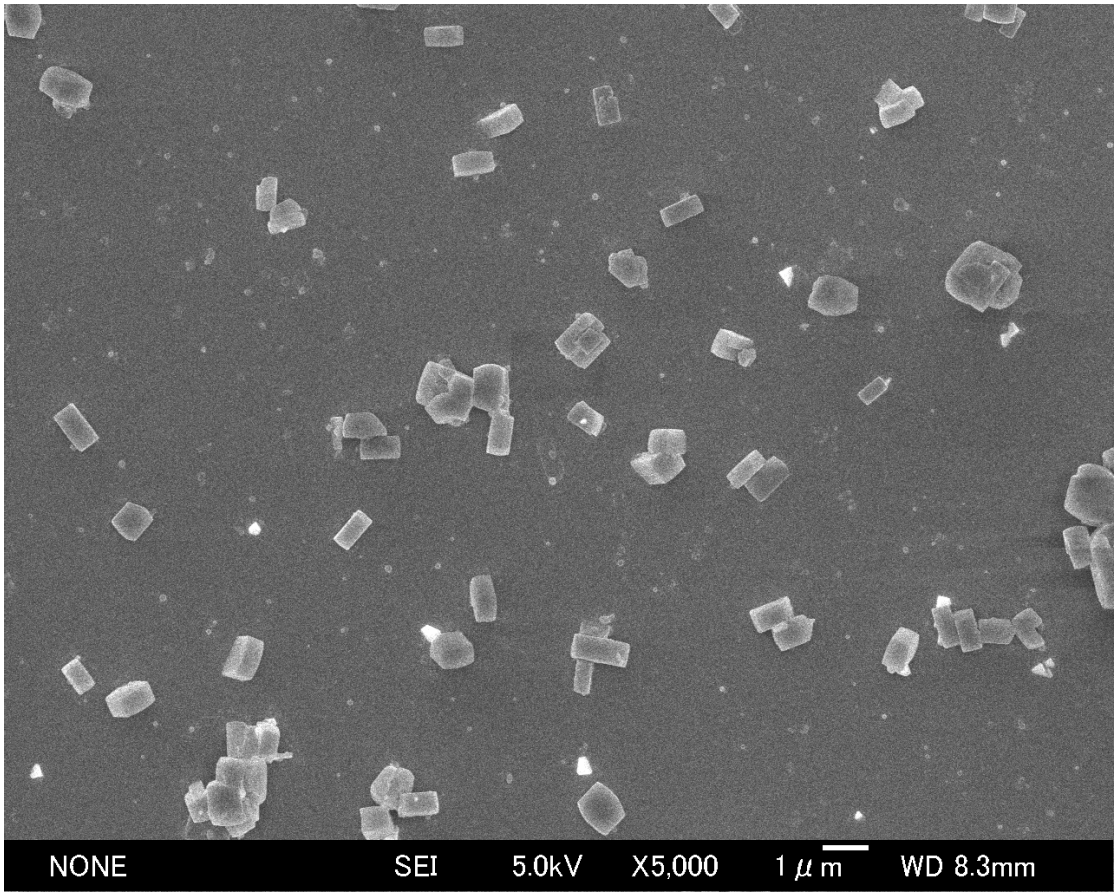

Figure 3-3.FE SEM of PPy-COF.

HR TEM of PPy-COF

HR TEM along 110 facet reveals the aligned 2D polymer sheets with face-to-face distance of about 3.4 Å (Fig.3-4), which is reasonable for π-π stack. These observations indicate that self-condensation of PDBA under solvothermal condition allows the formation of cube-like COF consisting of well-aligned polypyrene sheets.

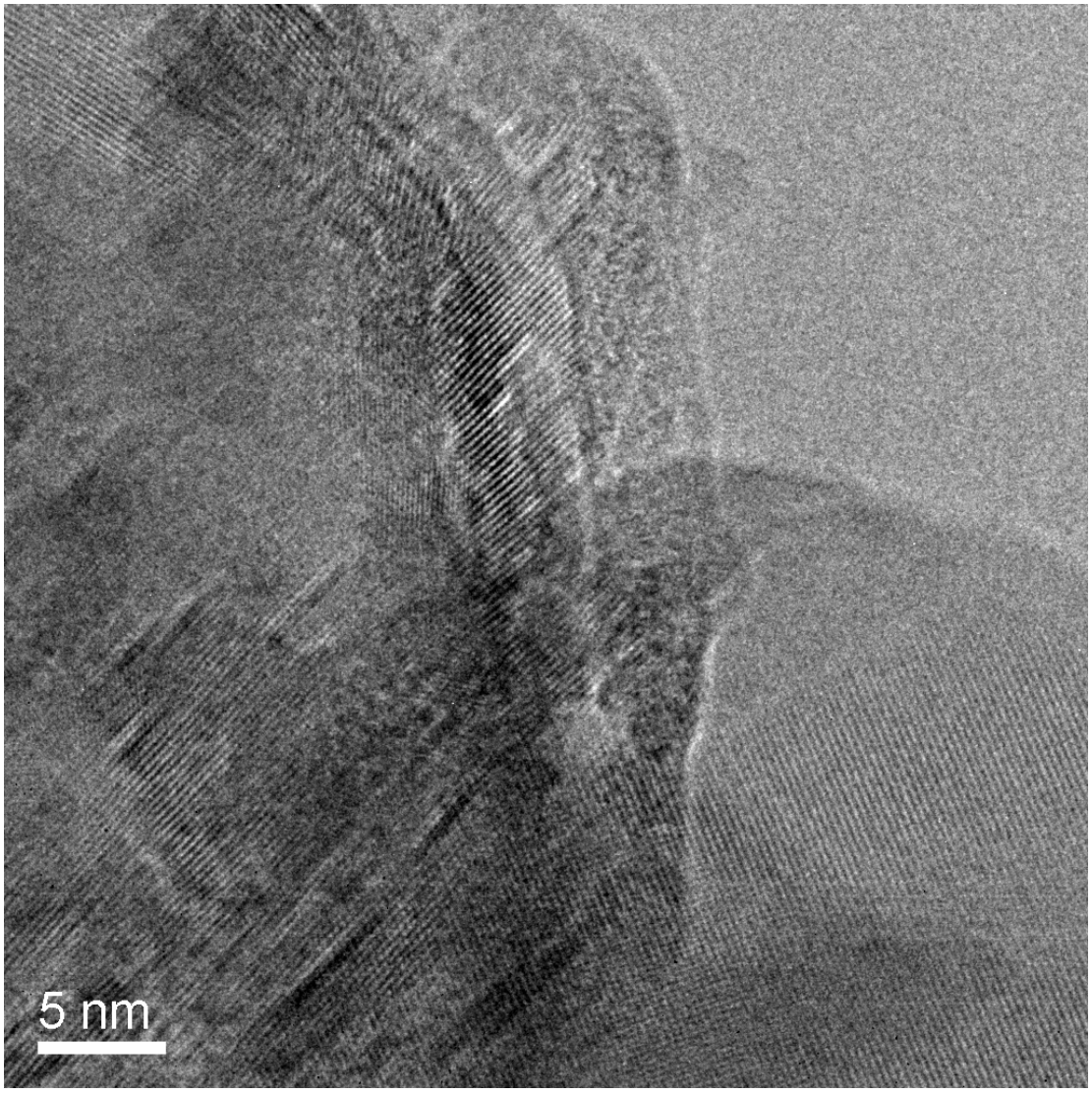

Figure 3-4.HR TEM of PPy-COF.

Experimental PXRD Pattern

PXRD measurement of PPy-COF displays a main peak at 4.6° due to 100 diffraction together with minor peaks at 9.3, 12.2 and 26.2° due to 200, 210, 001 diffractions, respectively (Fig.3-5, red curve).

Simulation of PXRD Pattern and Crystal Packing

To elucidate the lattice packing, we first carried out quantum chemical calculation with Gaussian 03. Rev. C01 at PM3 level to optimize the geometry of pore unit structure and then performed molecular modeling and Pawley refinement by using *Reflex*, a software package for crystal structure determination from the PXRD pattern, implemented in Materials Studio modeling version 4.2[7]. Simulation using *P*6/mmm space group with $a = b = 22.16295(838)$ Å and $c = 3.42066(165)$ Å results in a PXRD pattern (blue curve) that is in good agreement with the experimentally observed one (Fig. 3-5). On the other hand, simulation with *P*63/mmc space group gives a staggered alignment of 2D polymer sheets, where the calculated PXRD does not reproduce the experimental one (Fig. 3-6). Therefore, the 2D polypyrene sheets lay along *c* axis in a perfectly eclipsed fashion, with all vertices and edges superimposed on those from neighbouring sheet (Fig. 3-5), thus leaving aligned tubular channels with a pore diameter of 1.73 nm (Fig. 3-5).

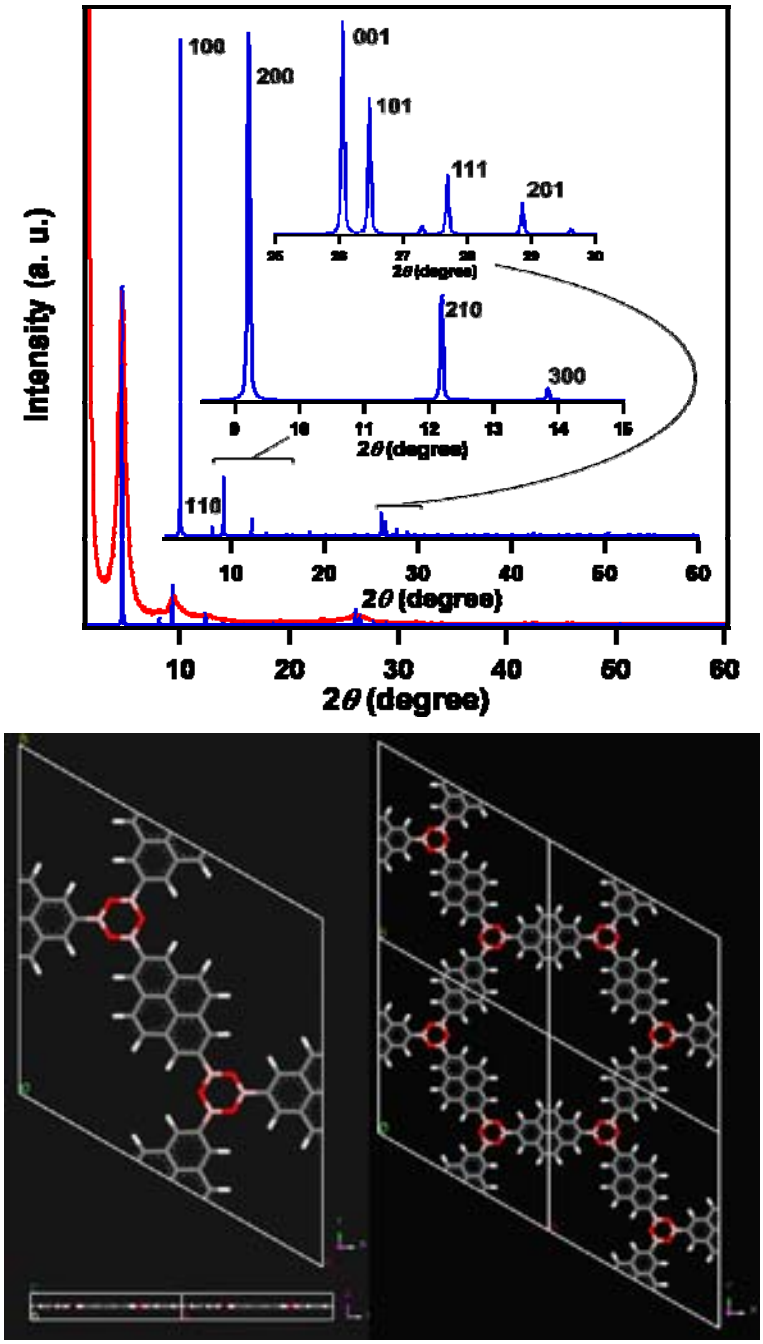

Figure 3-5.PXRD pattern of PPy-COF and simulation of crystal lattice packing in the eclipsed form. In the upper figure, the red curve represents the experimental PXRD pattern and the blue pattern is calculated from the eclipsed crystal packing (Crystal space group *P*6/mmm; No. 191). The calculated pattern simulates the experimental data well. The insets show the assignment of PXRD signals. The lower figure shows the eclipsed crystal lattice packing of PPy-COF. The pore size is 1.73 nm in diameter in the defined structure.

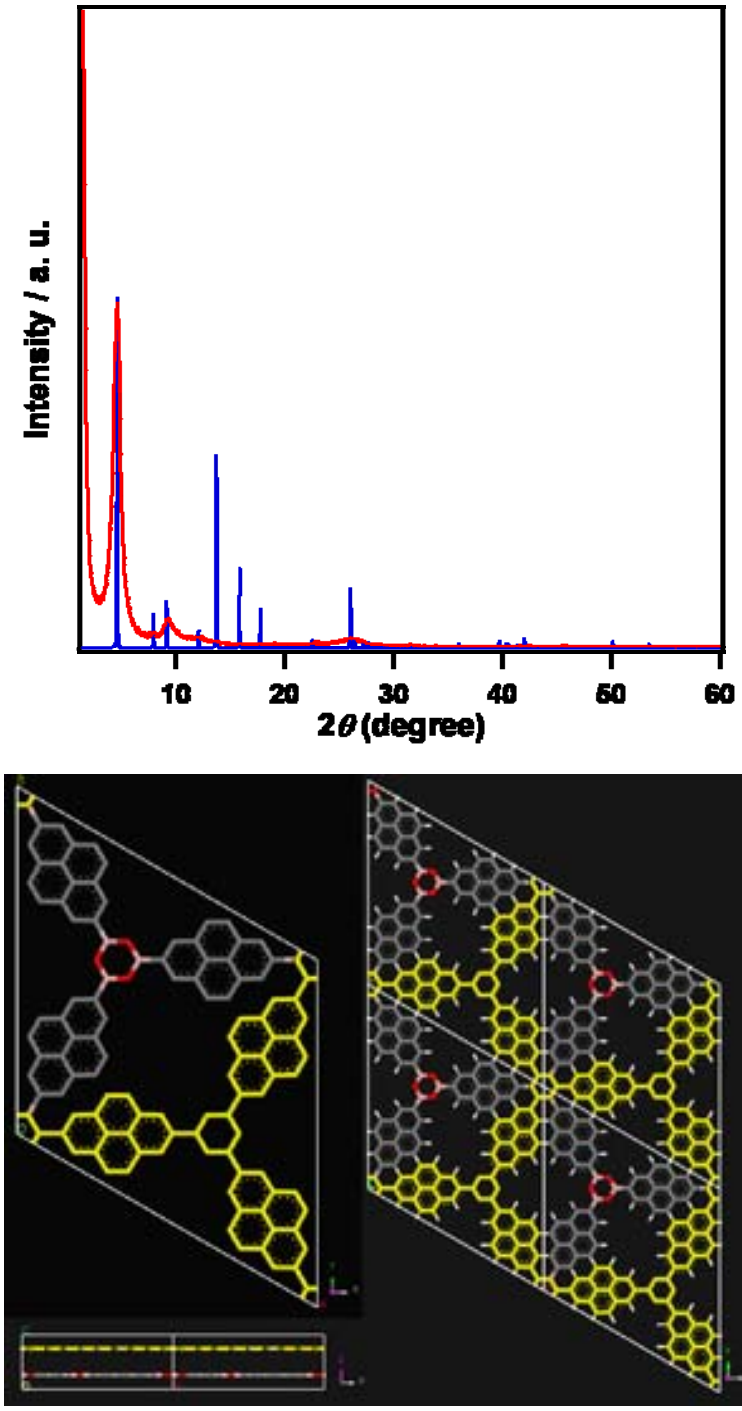

Figure 3-6.PXRD pattern of PPy-COF and simulation of crystal lattice packing in the staggered form. In the upper figure, the red curve represents the experimental PXRD pattern and the blue pattern is calculated from the staggered crystal packing (Crystal space group *P*63/mmc; No. 194). The simulated pattern does not fit the experimental data at all. The lower figure shows the staggered crystal lattice packing. In this case, the pore is covered and the pore size is significantly smaller than the experimental one.

Formula	$C_{48}H_{24}B_6O_6$
Formula weight	761.58
Crystal system	Hexagonal
Space group	*P*6/mmm (No.191)
Unit cell dimensions	$a = b = 22.16295(838)$ Å $c = 3.42066(165)$ Å
Cell volume	1453.12 $Å^3$
Density calculated	0.869 g/cm^3

Table 3-2: Refined crystal data

Atom	Wyck.	x	y	z
C1	12*q*	0.14521	0.62588	1/2
C2	12*q*	0.07328	0.59117	1/2
C3	12*q*	0.03489	0.62661	1/2
H4	12*q*	0.17408	0.68527	1/2
H5	12*q*	0.06339	0.68600	1/2
B6	6*m*	0.26177	0.63088	1/2
C7	6*m*	0.18206	0.59103	1/2
C8	6*m*	0.03650	0.51825	1/2
C9	6*m*	0.29791	0.59581	1/2

Table 3-3: Fractional atomic coordinate

Nitrogen Sorption Isotherm Measurement

Gas sorption measurement with N_2 at 77 K displays typical type-I sorption profile, suggesting a microporous character (Fig. 3-7a)[8]. The BET surface area was evaluated to be 923 m^2g^{-1} and the pore width was 1.88 nm calculated by NLDFT method (Fig. 3-7b), which is consistent with the theoretical one. These results indicate that PPy-COF is super microporous crystalline macromolecule with eclipsed alignment of polypyrene sheets.

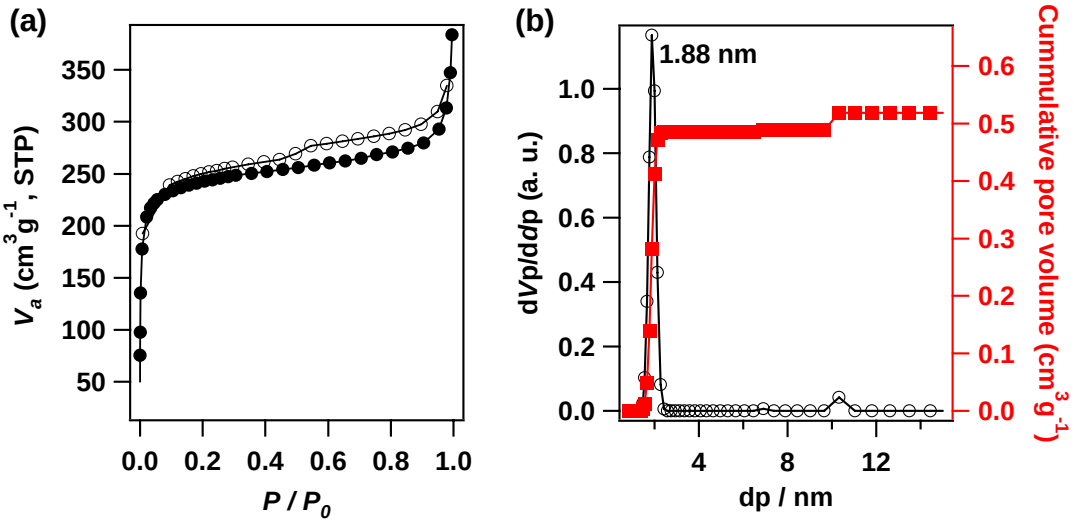

Figure 3-7.(a) Nitrogen adsorption (●) and desorption (○) isotherm profiles of PPy-COF at 77 K. (b) Pore size distribution of PPy-COF by DFT modeling on the N_2 adsorption isotherms.

Fluorescence Spectral Profiles

Fluorescence microscopy shows that PPy-COF is highly blue luminescent (Fig. 3-8a). Condensed poly(boronate ester)s bearing fluorene units have been reported as blue-emissive materials[9,10]. Fluorescence spectroscopy displays that upon excitation at 414 nm, PPy-COF emits a strong fluorescence at 484 nm (Fig. 3-8b, red curve). A control experiment with the simple solid of PDBA shows that the monomer unit gives

fluorescence centered at 421 nm (black curve). Therefore, the fluorescence of PPy-COF most likely originates from excimer, as a result of close packing of pyrene building blocks. The fluorescence quantum yield was evaluated to be about 5.8%, which is comparable to the reported value of pyrene (6.8%)[11].

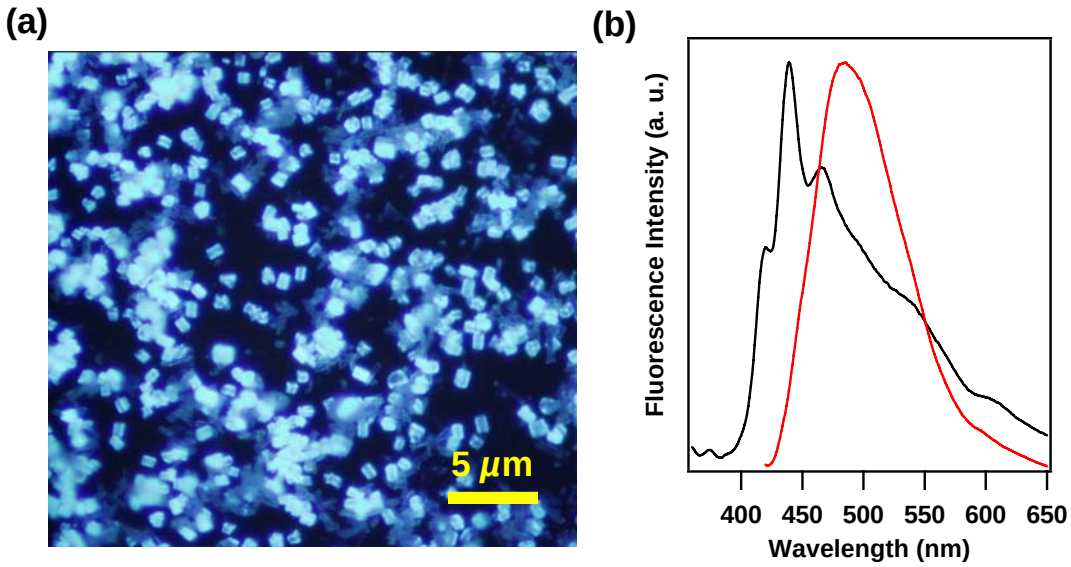

Figure 3-8.(a) Fluorescence image of PPy-COF. (b) Normalized fluorescence spectra of PPy-COF (red curve) and PDBA (black curve) upon excitation at 414 nm at 25 °C.

We also measured the excitation spectrum with diffuse reflectance UV-Vis spectrum of PPy-COF (Kubelka-Munk spectrum; shown in Fig. 3-9).

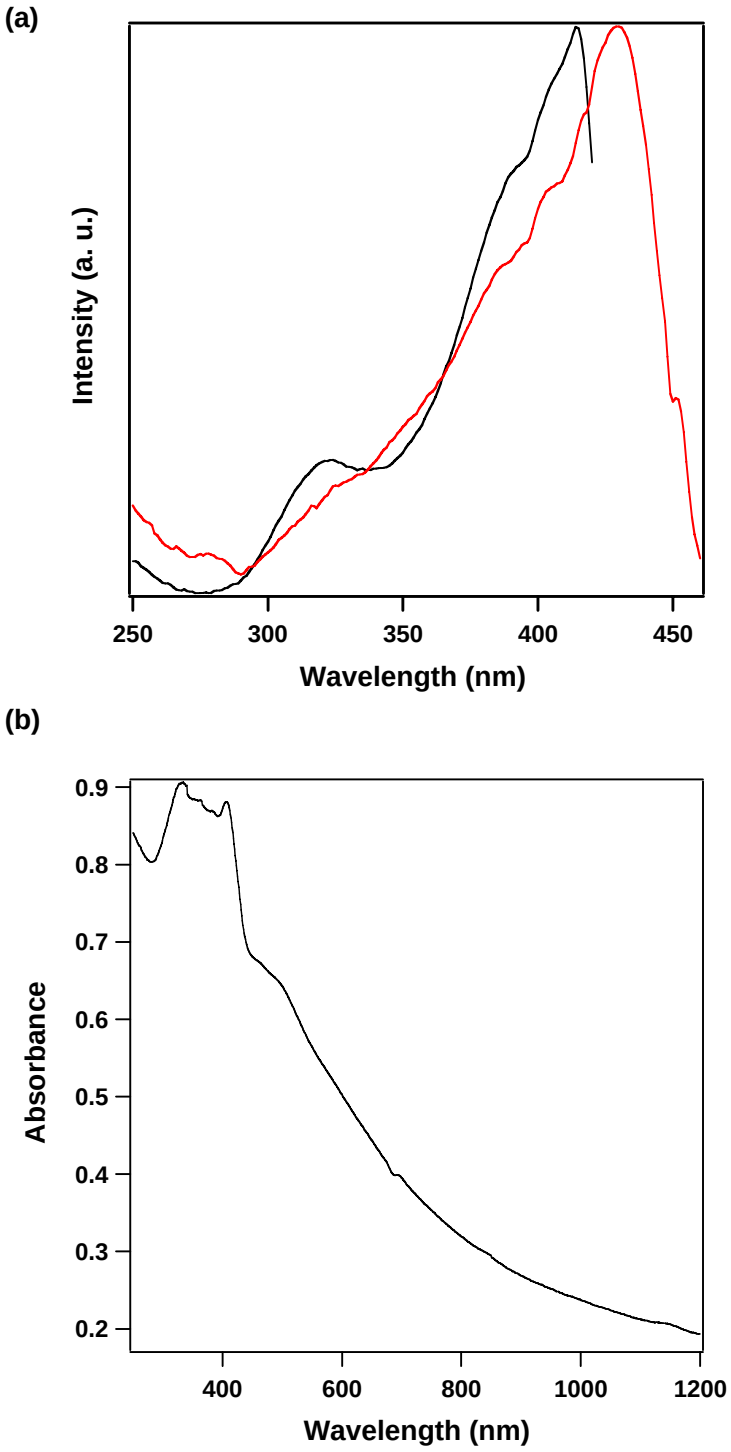

Figure 3-9.(a) Normalized fluorescence excitation spectra of PDBA (black curve) and PPy-COF (red curve). (b) Diffuse reflectance UV-VIS-NIR spectrum of PPy-COF.

Fluorescence Anisotropy of PPy-COF

Along this line, we further investigated the fluorescence anisotropy of PPy-COF upon excitation with a polarized light. When a chromophore with a restricted Brownian motion is excited by a polarized light, it emits a polarized fluorescence. However, the fluorescence should be depolarized when the excitation energy migrates randomly within the lifetime of the excited state. Here, fluorescence anisotropy (p) is defined by $(I_{||} - GI_{\perp})/(I_{||} + GI_{\perp})$,, where $I_{||}$ and $I_{\perp}$ are fluorescence intensities of parallel and perpendicular components relative to the polarity of the excitation light, respectively, where G is an instrumental correction factor. PDBA shows a p value of 0.018. In sharp contrast, PPy-COF under identical conditions exhibited a significantly depolarized fluorescence with an extremely low p value of 0.001. This observation reveals that the excitation energy is not localized but can migrate over the framework.

Semiconducting Property of PPy-COF

The ultimate π-stacking of pyrene building blocks in PPy-COF may have a high probability of becoming electrically semiconducting[12]. We measured the electrical conductivity by using a two-probe method across a 10-μm-width Pt gap. PPy-COF displays an almost linear I–V profile in air at 25 °C (Fig. 3-10a, blue curve), while the gap itself is silent, irrespective of voltage bias (Fig. 3-10a, black curve). In contrast, PDBA shows a low current under otherwise identical conditions (Fig. 3-11). Much interestingly, the electric current of PPy-COF can be on–off switched for many times without any deterioration (Fig. 3-10b). The relatively high electric conductivity is

clearly resulted from the highly aligned molecular order. Upon doping with iodine, the electric current increased (Fig. 3-10a, red curve), suggesting that PPy-COF is a *p*-type semiconductor.

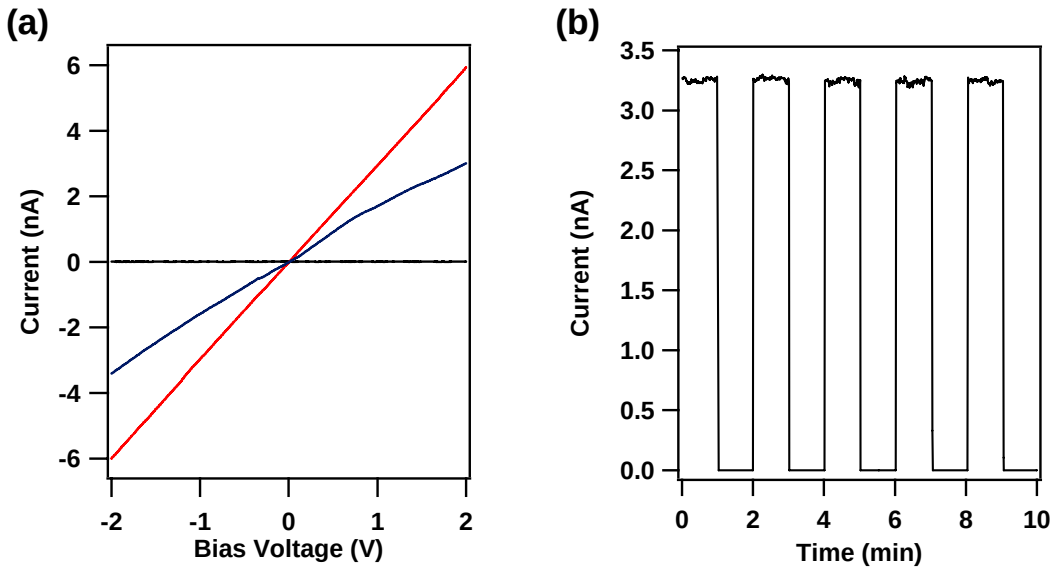

Figure 3-10.(a) I-V profile of PPy-COF between a 10-μm width Pt gap (black curve: without PPy-COF; blue curve: with PPy-COF; red curve: with iodine-doped PPy-COF). (b) Electric current when 2-V bias voltage is turned on or off.

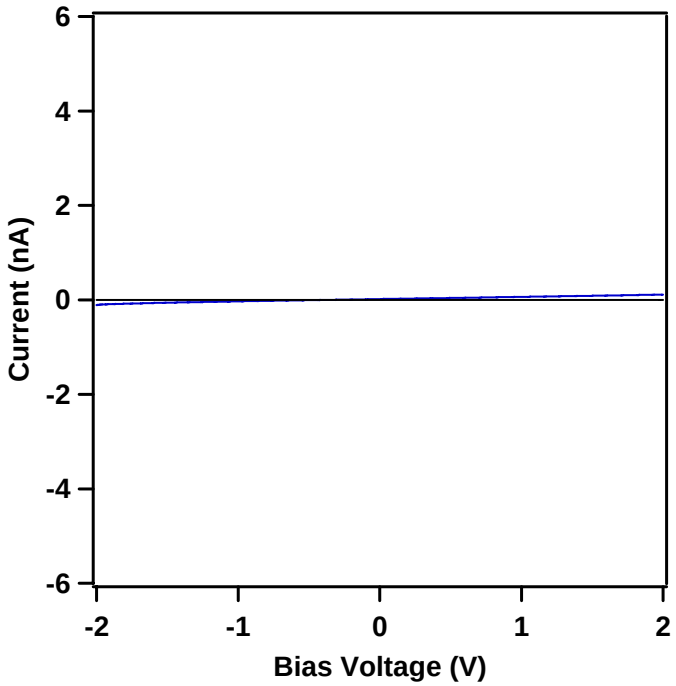

Figure 3-11. Electric conductivity of PDBA (blue curve) on 10-*u*m width Pt gap electrodes at 25 °C (black curve: electrodes only).

Photoconductivity of PPy-COF

Along this line, we investigated the photoconductivity of PPy-COF, since single crystal of pyrene has been reported to be photoconductive as a result of exciton migration across the lattice and charge separation at molecule-electrode interface[13,14]. PPy-COF shows a quick response to visible light irradiation (> 400 nm) and displays a linear I-V profile (Fig. 3-12). It is noticed that the photocurrent can be repetitively on-off switched for many times with a ratio large as 7.2×10^4 (Fig. 3-12b).

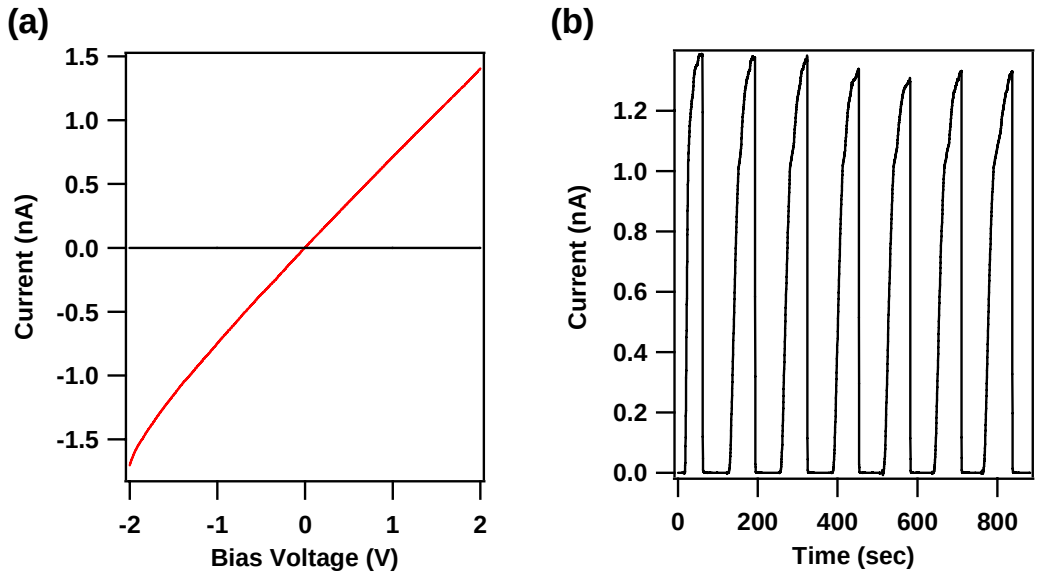

Figure 3-12.(a) I-V profile of PPy-COF between sandwich type Al/Au electrodes (black curve: without light irradiation; red curve: upon light irradiation). (b) Photocurrent when light is turned on or off.

3-4. Conclusion

In summary, the author demonstrated the synthesis of a new π-electronic COF based on self-condensation of pyrene diboronic acid under solvothermal condition. The ultimate alignment of 2D polypyrene sheets in a perfectly eclipsed fashion leads to the formation of micrometer-scale molecular cubes. PPy-COF is highly blue luminescent and allows exciton migration over the framework. PPy-COF is electrically semiconducting for hole transport. Moreover, PPy-COF is photoconductive to display quick response to light irradiation and is capable of repetitive on-off photocurrent switching. These unique properties clearly originate from the ultimate molecular ordering in COF and suggest a potential as optoelectronic material.

3-5. Experimental Section

Materials

THF was distilled over benzophenoneketyl under argon before use. Cyclohexane was distilled under argon before use. Pyrene, bispinacolatodiboron, anhydrous 1,4-dioxane (99.8%) and anhydrous acetone (99.8%) were purchased from Wako Chemicals. Mesitylene (98%) were purchased from TCI. 4,4'-di-*tert*-butyl-2,2'-bipyridine was purchased from Aldrich. Sodium periodate and hydrochloric acid were purchased from Kanto Co. Ltd. Methoxy(cyclooctadiene)iridium(I) dimer was purchased from Alfa Aesar Chemicals. Silica gel Wakogel C–300HG was used for column chromatography. Deuterated solvents for NMR measurements were obtained from Cambridge Isotope Laboratories, Inc. Pyrene-2,7-diboronic ester[15] and PDBA[9] were prepared according to reported methods.

Synthesis

All reactions were performed under argon using Schlenk line technique.

PPy-COF: A 1,4-dioxane/mesitylene (2.5 mL/2.5 mL) mixture of PDBA (25.0 mg, 0.345 mmol) in a 10-mLpyrextubewas degassed by three freeze-pump-thaw cycles, then the tube was sealed, kept in autoclave and heated at 120 °C for 2 days. The precipitate was collected by centrifugation, washed with anhydrous acetone and dried at 150 °C under vacuum to give PPy-COF (22 mg) as a pale yellow powder in 88% yield.

Measurements

^{1}H and ^{13}C NMR spectra were recorded on JEOL models JNM–LA400 or JNM–LA500 NMR spectrometers, where chemical shifts (δ in ppm) were determined with a residual proton of the solvent as standard. Infrared (IR) spectra were recorded on a JASCO model FT IR–6100 Fourier transform infrared spectrometer. UV-Vis-IR diffuse reflectance spectrum (Kubelka-Munk spectrum) was recorded on a JASCO model V-670 spectrophotometer equipped with integration sphere model IJN-727. Fluorescence spectroscopy was recorded on a JASCO model FP-6600 spectrofluorometer, while fluorescence quantum yield was estimated by dispersing PPy-COF in a PMMA/CH_2Cl_2 solution, with quinine sulfate as standard. Matrix–assisted laser desorption ionization time–of–flight mass (MALDI–TOF–MS) spectra were recorded on an Applied Biosystems BioSpectrometry model Voyager–DE–STR spectrometer in reflector or linear mode using 9–nitroanthracene or dithranol as matrix. Field emission scanning electron microscopy (FE SEM) was performed on a JEOL model JSM–6700 FE–SEM operating at an accelerating voltage of 1.5 or 5.0 kV. The sample was prepared by drop-casting an acetone suspension onto mica substrate and then coated with gold. Transmission Electron Microscope (TEM) images were obtained on a JEOL model JEM–3200 microscope. The sample was prepared by drop-casting an acetone suspension of TP-COF onto a copper grid. Powder X-ray diffraction (PXRD) data were recorded on a Rigaku model RINT Ultima III diffractometer by depositing powder on glass substrate, from $2\theta = 1.5°$ up to 60° with 0.02° increment at 25 °C.

Nitrogen sorption isotherms were measured at 77 K with a Bel Japan Inc. model BELSORP-mini II analyzer. Before measurement, the samples were degassed in vacuum at 200 °C for more than 6h. The Brunauer-Emmett-Teller (BET) method was utilized to calculate the specific surface areas. By using non-local density functional theory (NLDFT) model, the pore size was derived from the sorption curve.

Electrical measurements were carried out at 25 °C in air on PPy-COF or I_2-doped PPy-COF between 10-μm width Pt electrodes by a two-probe method using a Keithley model 2635 sourcemeter. PPy-COF was homogenously dispersed in acetone and casted onto the electrode to give a film. For I_2 doping, the PPy-COF electrode was kept in an I_2 atmosphere for 1h before measurement. As for the fabrication of devices for photo irradiation, PPy-COF was dispersed in PMMA/$CHCl_3$ (PPy-COF/PMMA = 50/50 wt%) to cast a thin film on Al electrode and Au electrode (30-nm thickness) was vapor deposited on the top of the film, to give a sandwich-type electrode gaps. PMMA was utilized as a glue to disperse PPy-COF homogenously since PMMA is free of any absorption in the irradiation wavelength region and has been widely utilized as standard glue for polymer samples in photo-generated carrier conductivity measurement[16]. The film thickness was about 100 μm as estimated by FE SEM measurement. A Xenon light source of Asahi Spectra MAX-301 model was utilized for the irradiation on the top of Au electrode. Due to the difference in electrode configurations, the observed currents are not comparable for those using Pt gap electrodes and sandwich-type Al/Au electrodes.

Geometry optimization of the unit pore structure was performed at PM3 level by using the Gaussian 03 program package (Revision C.02)[17] to give the pore size of 1.73 nm in diameter. Geometry optimization of the repeating unit was performed at B3LYP/6-31G(d) level by using the Gaussian 03 program package in order to make unit cell structure. The final molecular structure in a hexagonal unit cell was prepared by using geometrical parameters from the optimized structure. Molecular modeling and Pawley refinement were carried out using Reflex, a software package for crystal determination from PXRD pattern, implemented in MS modeling ver 4.2 (Accelrys Inc.)[7]. Unit cell dimension was first manually determined from the observed PXRD peak positions by using hexagonal arrangement. We performed Pawley refinement to optimize the lattice parameters iteratively until the RWP value converges. The refinement indicates a hexagonal crystal system with a unit cell of $a = b =$ 22.16295(838) Å and c = 3.42066(165) Å. The pseudo-Voigt profile function was used for whole profile fitting and Berrar-Baldinozzi function was used for asymmetry correction during the refinement processes. The final RWP and RP values were 8.10% and 5.64%, respectively. Simulated PXRD patterns were calculated from the refined unit cell and compared with the experimentally observed patterns. This structure could have two distinct arrangements: (1) a staggered AB type arrangement with graphite-like packing, where three-connected vertices lie over the center of the six-membered rings of neighboring layers; (2) an eclipsed AA type arrangement, where all atoms in an each layer of the framework lie exactly over one another. The AA type arrangement was constructed in space group *P*6 symmetry (space group number 191)

and the AB type arrangement was constructed in space group *P*63/mmc symmetry (space group number 194). The atoms are placed on the special position to form the 2D framework where all bond lengths and angles are taken from the optimized geometrical parameters calculated at B3LYP/6-31G(d) to maintain reasonable values. After comparing each simulated pattern with experimentally observed pattern, only the simulated pattern from the eclipsed AA type arrangement shows good agreement with the observed PXRD pattern.

3-6. References

1. A. P. Côté, A. I. Benin, N. W. Ockwig, M. O'Keeffe, A. J. Matzger, O. M. Yaghi, *Science* **2005**, *310*, 1166-1170.
2. H. M. El-Kaderi, J. R. Hunt, J. L. Mendoza-Cortés, A. P. Côté, R. E. Taylor, M. O'Keeffe, O. M. Yaghi, *Science* **2007**, *316*, 268-272.
3. A. P. Côté, H. M. El-Kaderi, H. Furukawa, J. R. Hunt, O. M. Yaghi, *J. Am. Chem. Soc.***2007**, *129*, 12914-12915.
4. R. W. Tilford, W. R.Gemmill, H. C. zur Loye, J. J. Lavigne, *Chem. Mater.* **2006**, *18*, 5296-5301.
5. R. W. Tilford, S. J. Mugavero III, P. J. Pellechia, J. J. Lavigne, *Adv. Mater.* **2008**, *20*, 2741-2746.
6. S. Wan, J. Guo, J. Kim, H. Ihee, D. Jiang, *Angew. Chem. Int. Ed.* **2008**, *47*, 8826-8830.

7. Accelrys, Material Studio Release Notes, Release 4.2, Accelrys Software, San Diego 2006.

8. K. M. Sing, D. H. Everett, R. A. W. Haul, L. Moscou, R. A. Pierotti, J. Rouquerol, T. Siemieniewska, *Pure & Appl. Chem.***1985**, *57*, 603-619.

9. W. Niu, M. D. Smith, J. J. Lavigne, *J. Am. Chem. Soc.* **2006**, *128*, 16466-16467.

10. Y. Li, J. Ding, M, Day, Y. Tao, J. Lu, M. D'iorio, *Chem. Mater.* **2003**, *15*, 4936-4943.

11. J. Shirel, A. Penzkofer, R. Procházka, Z. J. Shen, Strauss, J. Daub, *Chem. Phys.* **2007**, *331*, 427-437.

12. J. M. Warman, M. P. de Haas, G. Dicker, F. C. Grozema, J. Piris, M. G. Debije, *Chem. Mater.* **2004**, *16*, 4600-4609.

13. M. Tierney, D. Lubman, *Appl. Spectr.* **1987**, *41*, 880-886.

14. H. Inokuchi, *Bull. Chem. Soc., Jpn.* **1956**, *29*, 131-133.

15. C. C. Tzschucke, J. M. Murphy and J. F. Hartwig, *Org. Lett.* **2007**, *9*, 761-764.

16. A. Acharya, S. Seki, Y. Koizumi, A. Saeki, and S. Tagawa, *J. Phys. Chem. B* **2005**, *109*, 20174-20179.

17. Gaussian 03, Revision C.02, Frisch, M. J.; Trucks, G. W.; Schlegel, H. B.; Scuseria, G. E.; Robb, M. A.; Cheeseman, J. R.; Montgomery, Jr., J. A.; Vreven, T.; Kudin, K. N.; Burant, J. C.; Millam, J. M.; Iyengar, S. S.; Tomasi, J.; Barone, V.; Mennucci, B.; Cossi, M.; Scalmani, G.; Rega, N.; Petersson, G. A.; Nakatsuji, H.; Hada, M.; Ehara, M.; Toyota, K.; Fukuda, R.; Hasegawa, J.; Ishida, M.; Nakajima, T.; Honda, Y.; Kitao, O.; Nakai, H.; Klene, M.; Li, X.; Knox, J. E.; Hratchian, H. P.; Cross, J.

B.; Bakken, V.; Adamo, C.; Jaramillo, J.; Gomperts, R.; Stratmann, R. E.; Yazyev, O.; Austin, A. J.; Cammi, R.; Pomelli, C.; Ochterski, J. W.; Ayala, P. Y.; Morokuma, K.; Voth, G. A.; Salvador, P.; Dannenberg, J. J.; Zakrzewski, V. G.; Dapprich, S.; Daniels, A. D.; Strain, M. C.; Farkas, O.; Malick, D. K.; Rabuck, A. D.; Raghavachari, K.; Foresman, J. B.; Ortiz, J. V.; Cui, Q.; Baboul, A. G.; Clifford, S.; Cioslowski, J.; Stefanov, B. B.; Liu, G.; Liashenko, A.; Piskorz, P.; Komaromi, I.; Martin, R. L.; Fox, D. J.; Keith, T.; Al-Laham, M. A.; Peng, C. Y.; Nanayakkara, A.; Challacombe, M.; Gill, P. M. W.; Johnson, B.; Chen, W.; Wong, M. W.; Gonzalez, C.; and Pople, J. A.; Gaussian, Inc., Wallingford CT, 2004.

Chapter 4

An Anthracene–Based Photo-Addressable Covalent Organic Framework

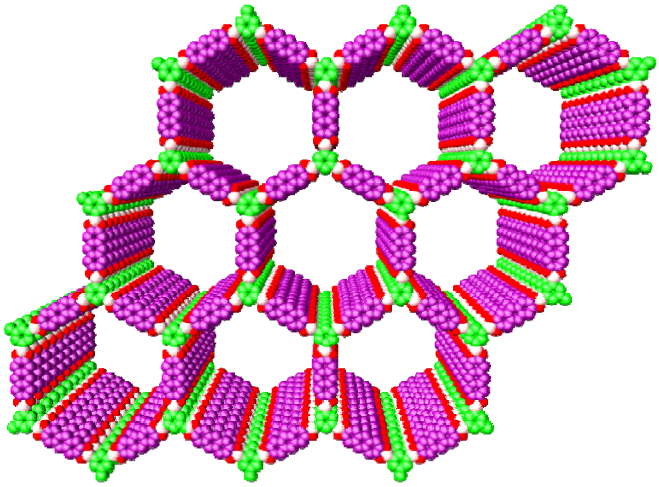

4-1. Abstract

In this part, the author disclosed the design and synthesis of a new type of COF based on co-condensation of benzene triboronic acid and 2,3,6,7-tetrahydroxyanthracene under solvothermal or reflux conditions (An-COF). An-COF consists of benzene and anthracene components alternatively linked in a mesoporous hexagonal skeleton. FE SEM reveals that An-COF adopts well-defined micrometer-scaled 2D sheet shape. Moreover, An-COF is electrically semiconducting and highly luminescent. The ultimate alignment of An-COF sheets in a perfectly eclipsed fashion allows photo-induced dimerization and reversible monomerization of anthracene units in An-COF. Such a photo-addressable COF may find applications in tuning luminescence and high-density data storage.

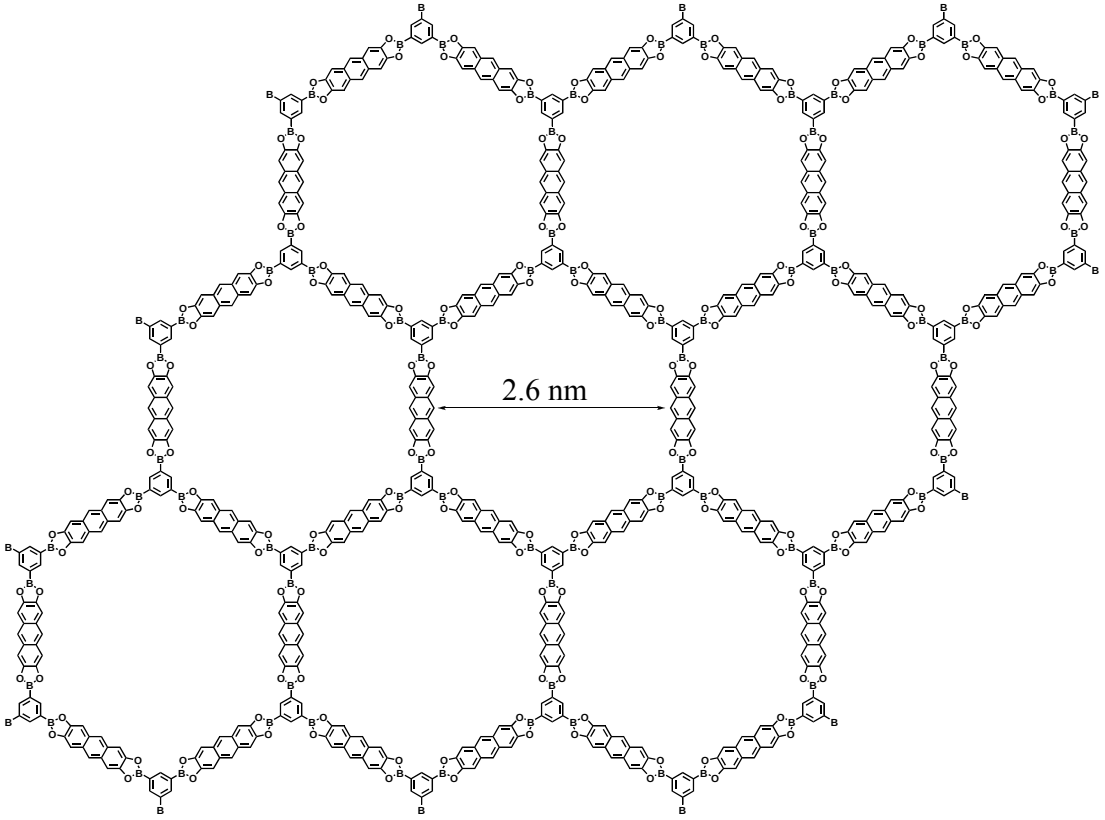

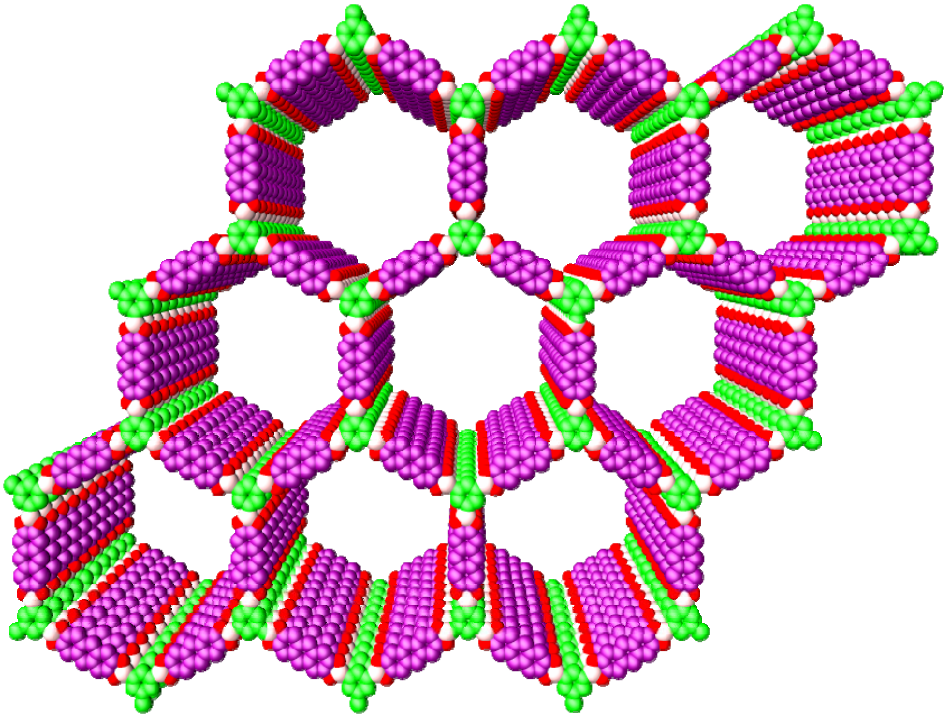

Figure 4-1. Schematic representation of An-COF.

4-2. Design of An-COF

An-COF was topologically designed by employing a D_{3h} symmetric monomer as corner and a D_{2h} symmetric monomer as edge for pore hexagons and synthesized by a condensation reaction of 1,3,5-benzene triboronic acid (BTBA) and 2,3,6,7-Tetrahydroxyanthracene (THA).

2-3. Synthesis and Characterization of An-COF

Synthesis of An-COF

In a typical experiment, THA (24.3 mg, 0.1mmol) and BTBA (17.5 mg, 0.066mmol) were mixed in 1,4-dioxane/mesitylene (1.5mL/1.5mL) in a 10-mL pyrex tube was degassed by three freeze-pump-thaw cycles. Then the tube was sealed, kept

in autoclave and heated at 120 °C for 3 days[1]. The precipitate was collected by centrifugation, washed with anhydrous acetone, and dried at 150 °C under vacuum to give An-COF (31 mg) as a green black powder in 81% yield.

FT IR Spectral Profiles

FT IR spectroscopy shows that vibrational bands due to boronic ester ring appeared at 1327, 1306, 1229, and 1040 cm^{-1}, whereas the hydroxyl bands of the starting materials were strongly attenuated in An-COF, indicating the condensation of two monomers (Fig. 4-2, Table 4-1).

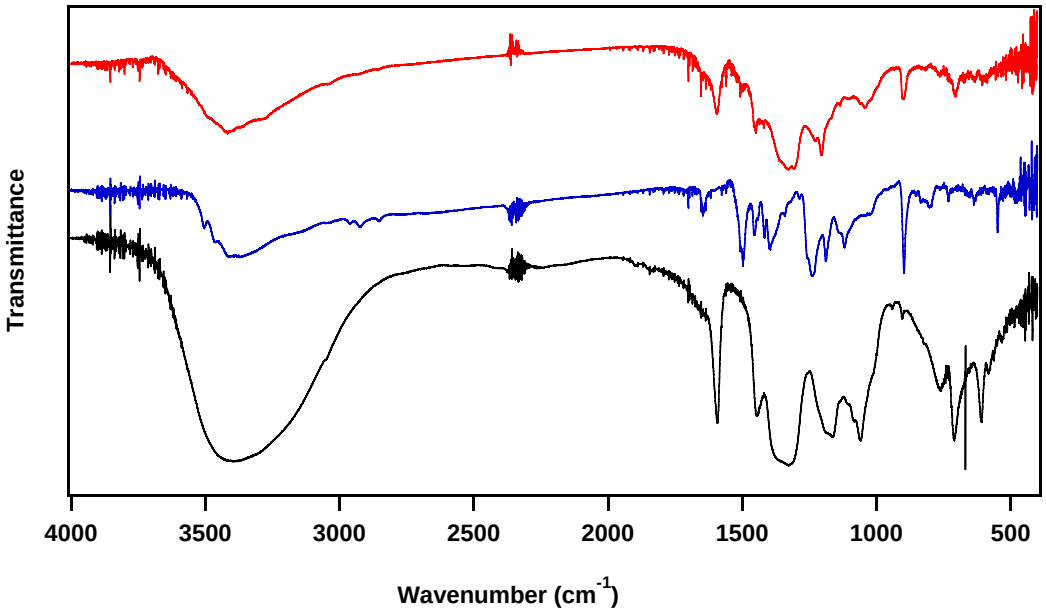

Figure 4-2.FT IR spectra of BTBA, THA and An-COF. The red, blue and black curves are IR spectra of An-COF, BTBA and THA, respectively.

Peak (cm^{-1})	**Assignment and Notes**
3416.76 (m)	O–H stretch from the end $B(OH)_2$ or OH groups
3037.58 (w)	Aromatic C–H stretch from benzene units
2928.86 (w)	C–H stretching from anthracene building blocks
1594.36 (m)	C=C vibrational mode of phenyl ring. Characteristic band
1450.93 (m)	C=C vibrational modes for anthracene building block
1326.79 (s)	B–O stretch, characteristic band for boroxoles
1306.30 (s)	B–O stretch
1229.40 (s)	C–O stretch, characteristic for boroxoles
1169.13 (m)	C–H in-plane bending modes
1132.97 (m)	
1040.17 (m)	B–C stretch
898.91 (m)	C–H out-of-plane bending modes
776.08 (m)	
704.61 (m)	

Table 4-1: Peak assignments for FT-IR spectrum of An-COF.

FE SEM of An-COF

FE SEM images of An-COF reveal that the condensation polymerization of BTBA and THA affords sheets with length and width extended to micrometers (Fig. 4-3), and no other morphologies are observable (Fig. 4-4).

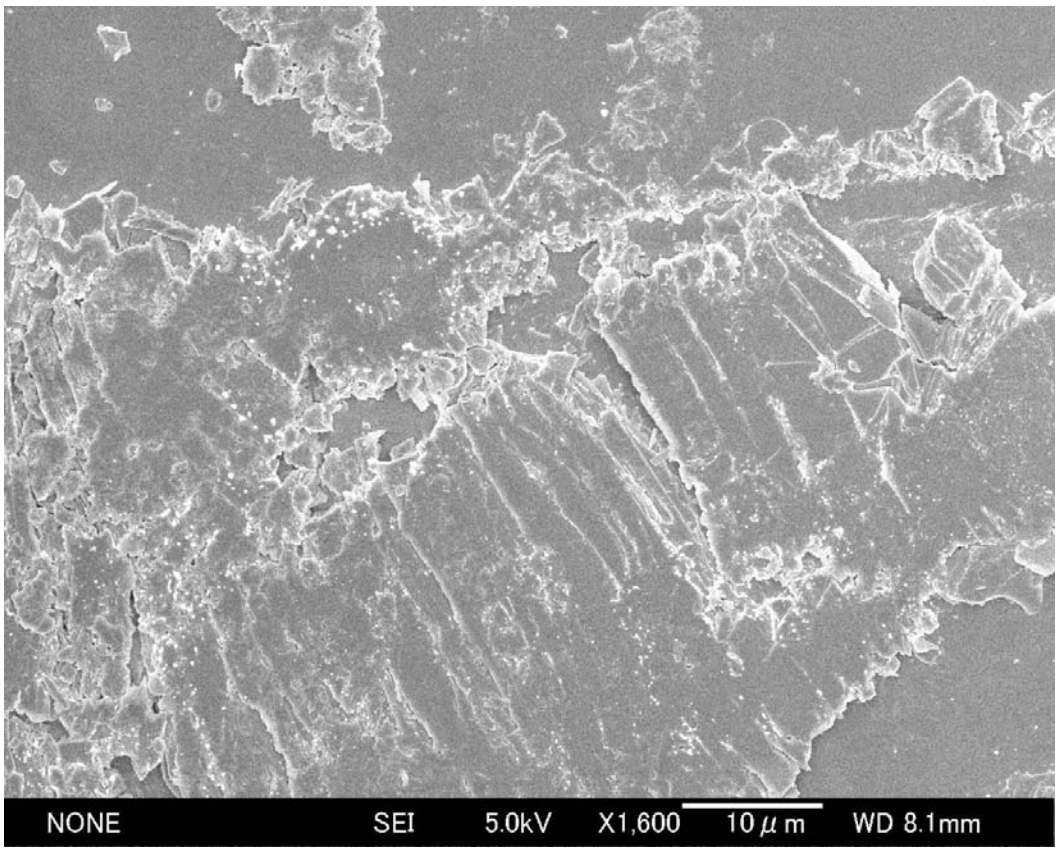

Figure 4-3.FE SEM of An-COF.

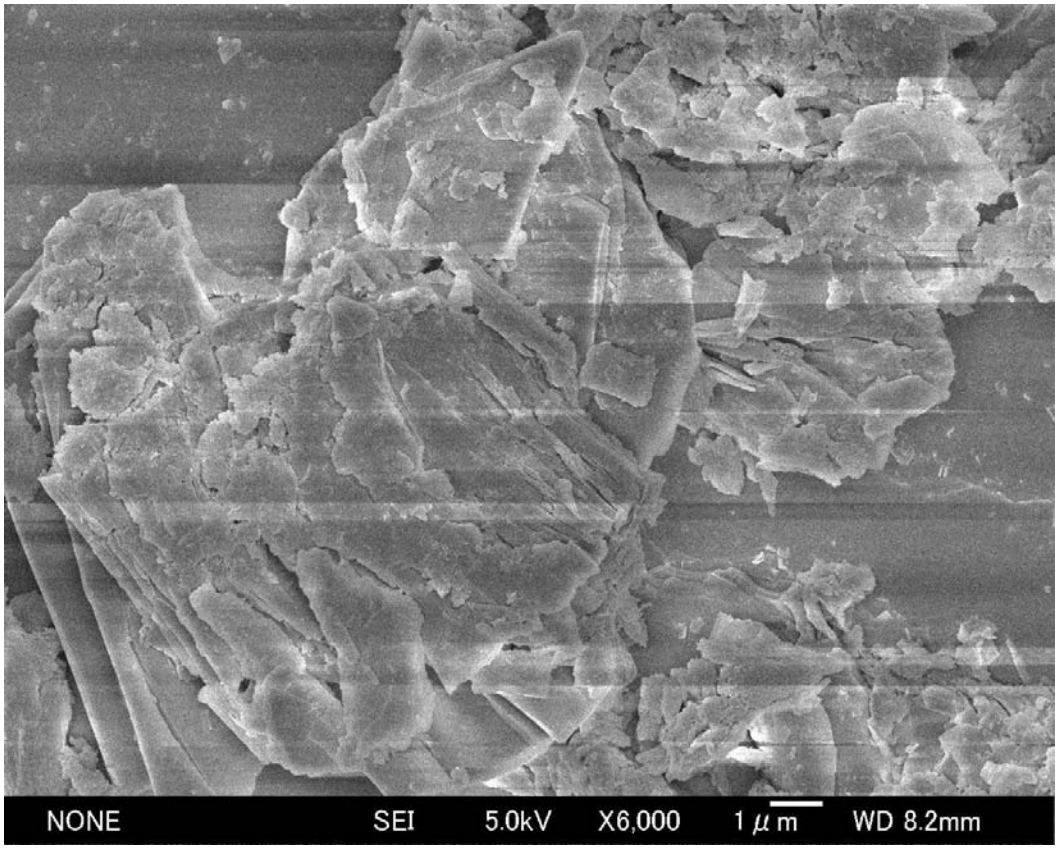

Figure 4-4.FE SEM of An-COF.

HR TEM of An-COF

To further investigate the structure, high resolution TEM was performed. As shown in Figure 4-5, clear aligned patterns were observed along the (110) facet. From the aligned layer structure, the distance between sheets is estimated to be 3.40 Å, which is reasonable for π-π stacking (Fig. 4-5). Moreover, along the (001) facet, hexagonal mesostructure can also be observed and enables the estimation of center-to-center distance between the neighbouring pores to be about 2.6 nm (Fig.4-6, 4-7).

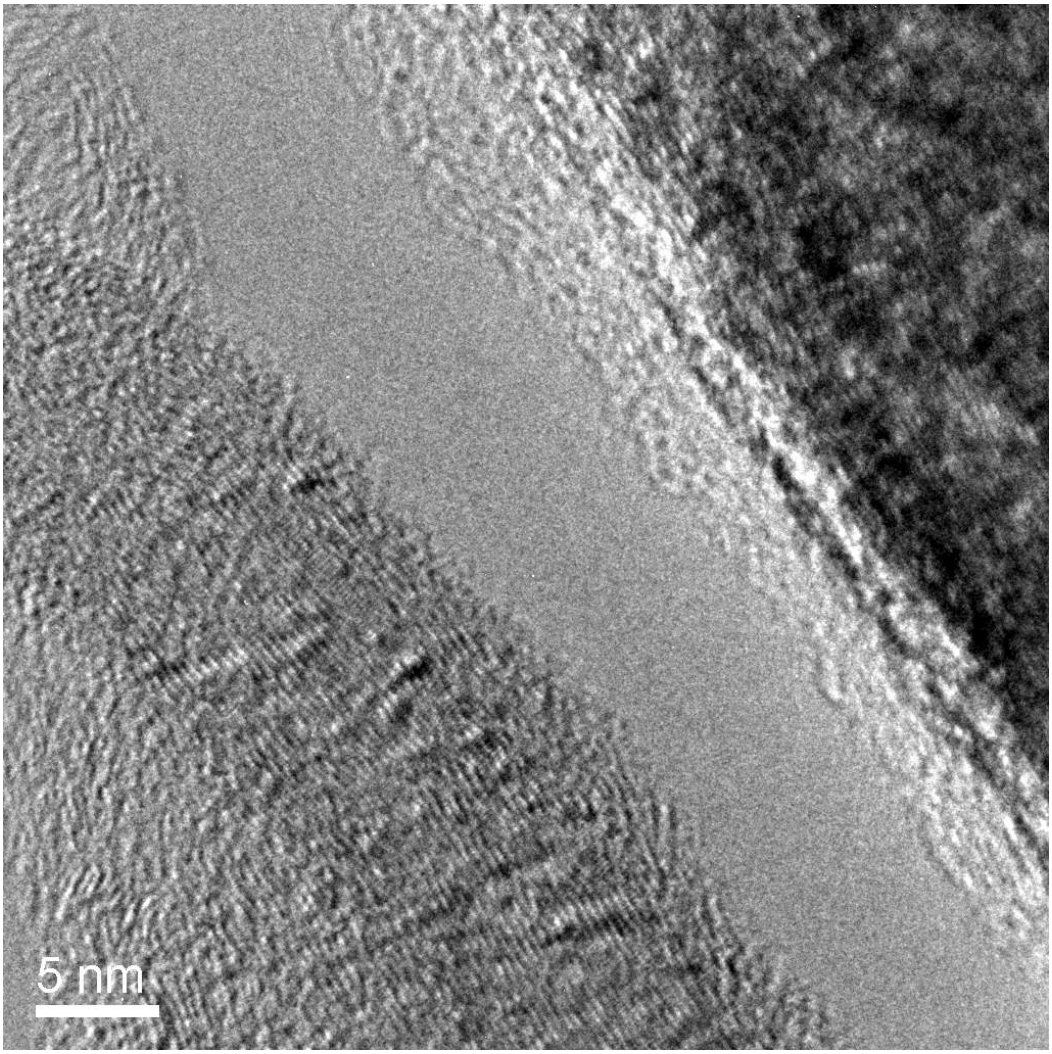

Figure 4-5.HR TEM of An-COF.

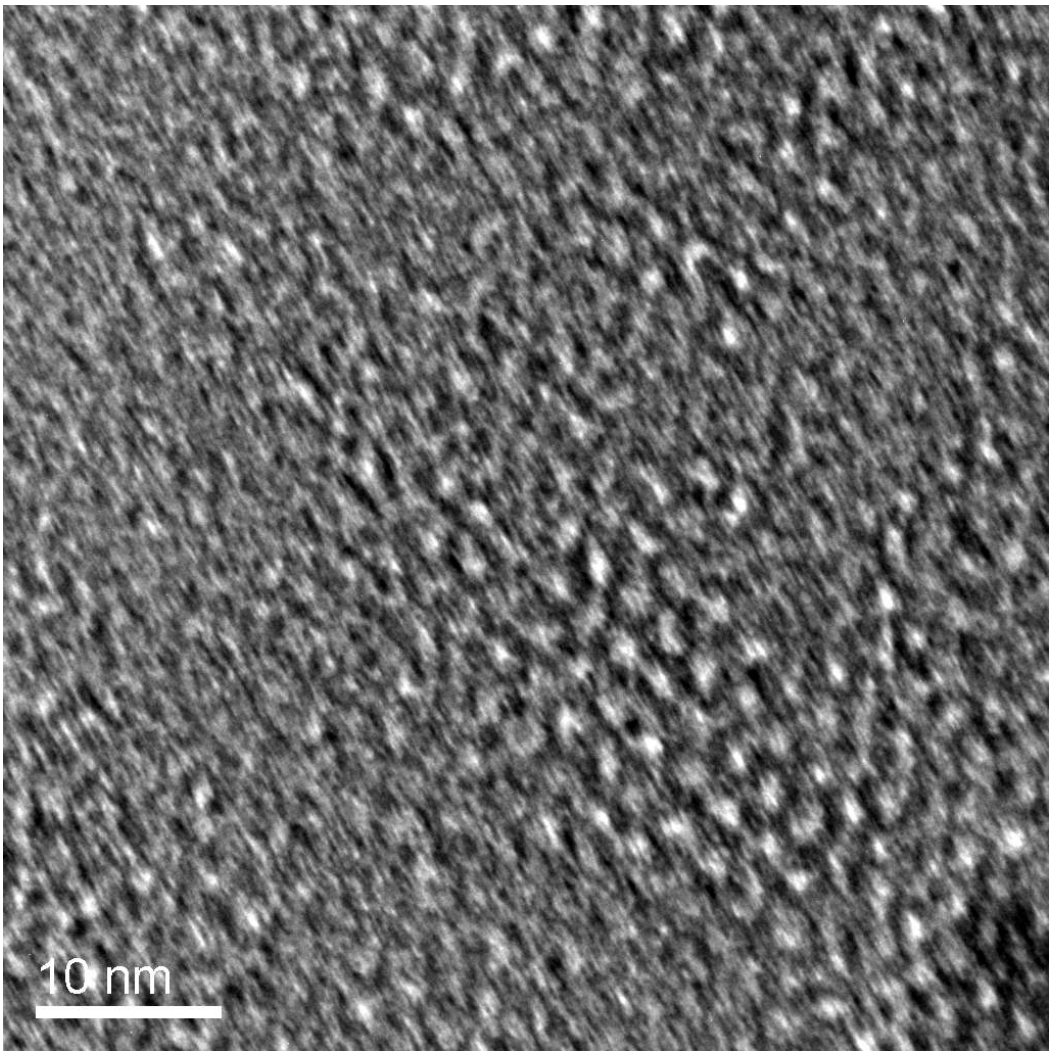

Figure 4-6.HR TEM of An-COF.

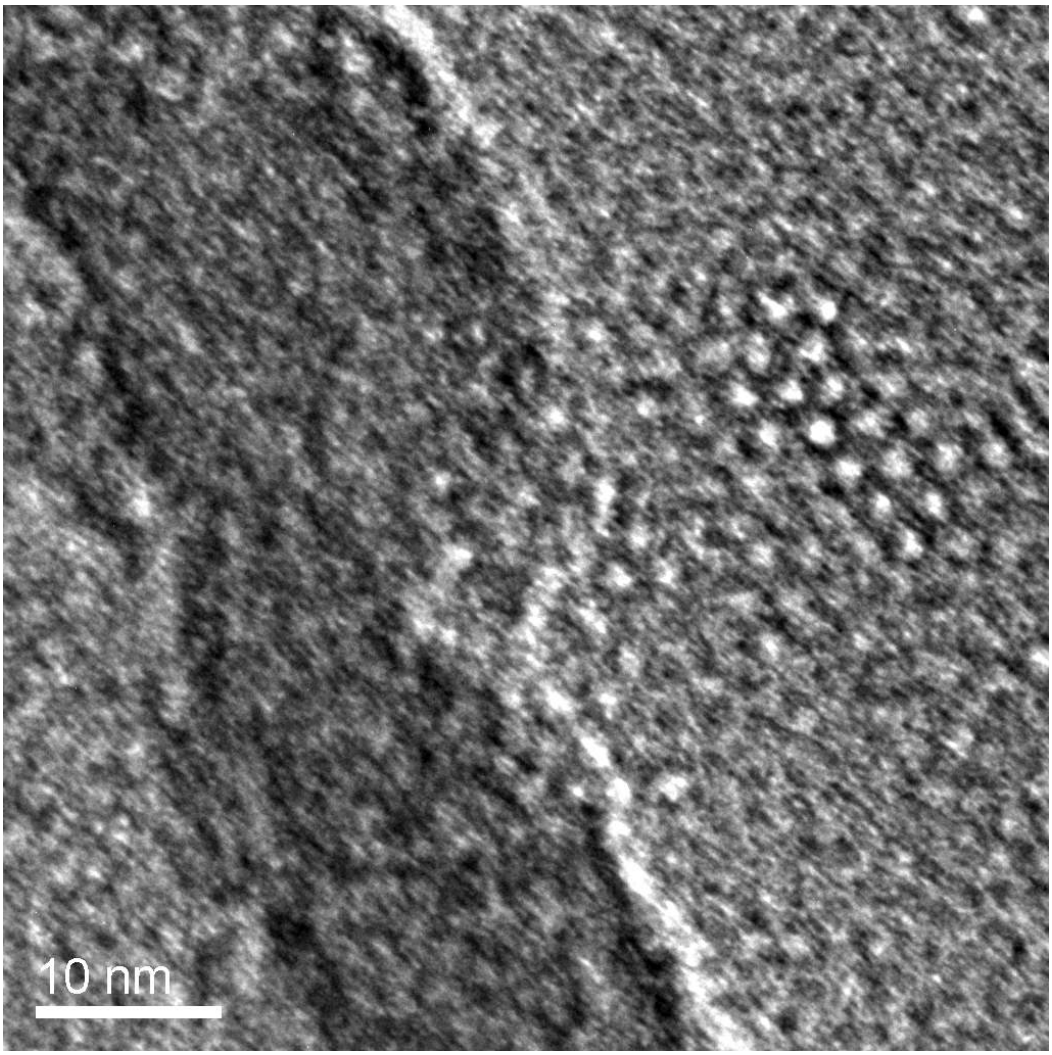

Figure 4-7.HR TEM of An-COF.

Experimental PXRD Pattern

Powder x-ray diffraction (PXRD) exhibits a main diffraction peak due to 100 at 3.36°, along with diffractions owing to 110, 200, 210, and 001 at 5.96°, 6.88°, 9.20° and 26.54°, respectively (Figure 4-8, red curve).

Simulation of PXRD Pattern and Crystal Packing

To elucidate the lattice packing, we first carried out semi-empirical calculation at PM3 level to optimize the geometry of the whole pore unit structure and further optimized the molecular geometry of the repeating unit in the single unit cell at B3LYP/6-31G(d) by using Gaussian 03 program[2]. Final lattice parameters were determined after performing Pawley refinement by using Reflex, a software package for crystal structure determination from the PXRD pattern, implemented in MS modelling (ver4.2)[3]. Simulation using the space group of *P*6/mmm (No. 191) with $a = b = 30.33032$ Å and $c = 3.36227$ Å gives a PXRD pattern in good agreement with the experimentally observed one (Fig. 4-8). All the diffraction peaks can be reasonably assigned. On the other hand, a staggered model using the space group of *P*63/mmc (No. 194) does not reproduce the experimental PXRD pattern (Fig. 4-9). Therefore, the 2-D sheets crystallize in an eclipsed fashion to give a perfect superimposition of the triphenylene and pyrene units on themselves (Fig. 4-1, Fig. 4-8). Such a crystalline structure would provide open and aligned mesopores of 2.6 nm in diameter (Fig. 4-8).

Simulation and Calculation of Crystal Lattice Packing

Formula	$C_{54}O_{12}B_6$
Formula weight	905.44
Crystal system	Hexagonal
Space group	*P*6/mmm (No.191)
Unit cell dimensions	$a = b = 30.33032$ Å $c = 3.36227$ Å
Cell volume	2678.66 $Å^3$
Density calculated	0.601505 g/cm^3

Table 4-2. Refined crystal data

Atom	Wyck.	x	y	z
B1	12*q*	0.21964	0.60947	0.50000
O2	12*q*	0.18960	0.55612	0.50000
C3	12*q*	0.13934	0.54594	0.50000
C4	12*q*	0.09536	0.49902	0.50000
C5	12*q*	0.04736	0.49956	0.50000
C6	6*m*	0.27892	0.63946	0.50000
C7	6*m*	0.30677	0.69323	0.50000

C8	6*k*	0.54631	0.54631	0.50000

Table 4-3. Fractional atomic coordinate

Simulation of PXRD Pattern and Crystal Packing

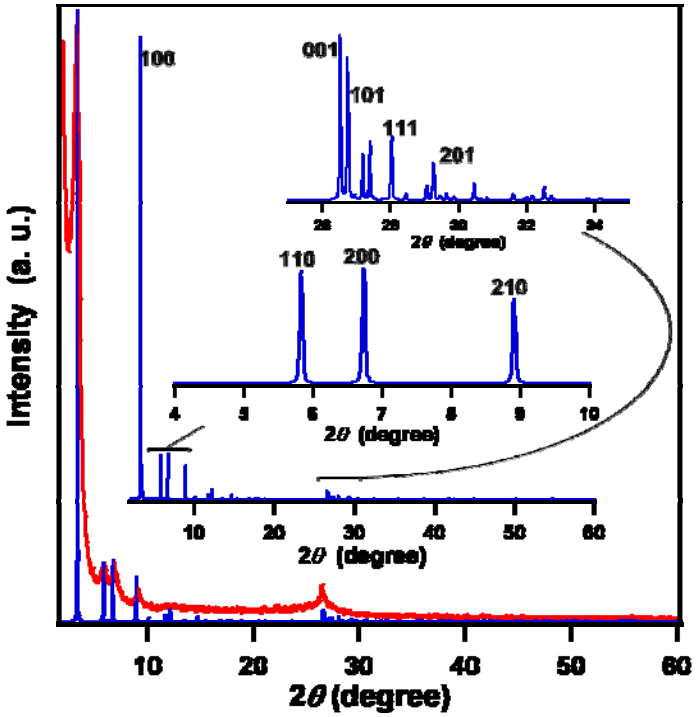

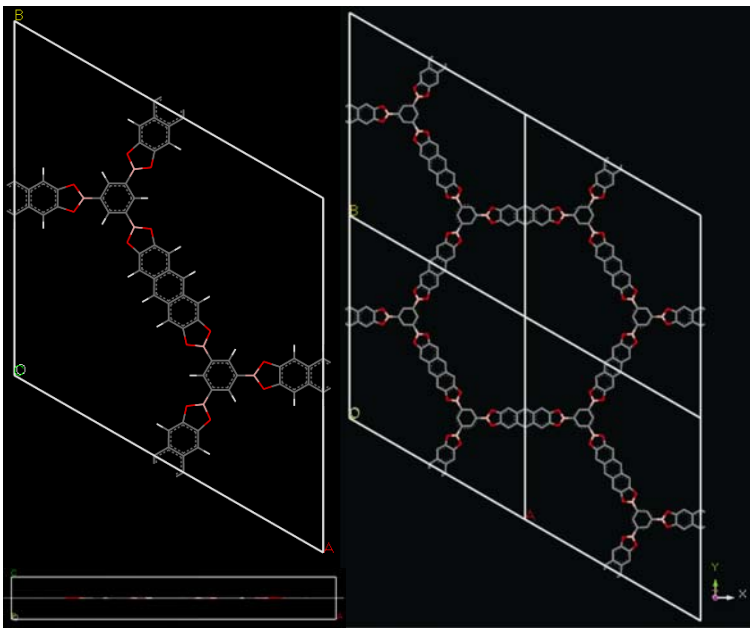

Figure 4-8.PXRD pattern of An-COF and simulation of crystal lattice packing in the eclipsed form. In the upper figure, the red curve represents the experimental PXRD pattern and the blue pattern is calculated from the eclipsed crystal packing (Crystal space group *P*6/mmm; No. 191). The

calculated pattern simulates the experimental data well. The insets show the assignment of PXRD signals. The lower figure shows the eclipsed crystal lattice packing of An-COF. The pore size is 2.74 nm in diameter in the defined structure.

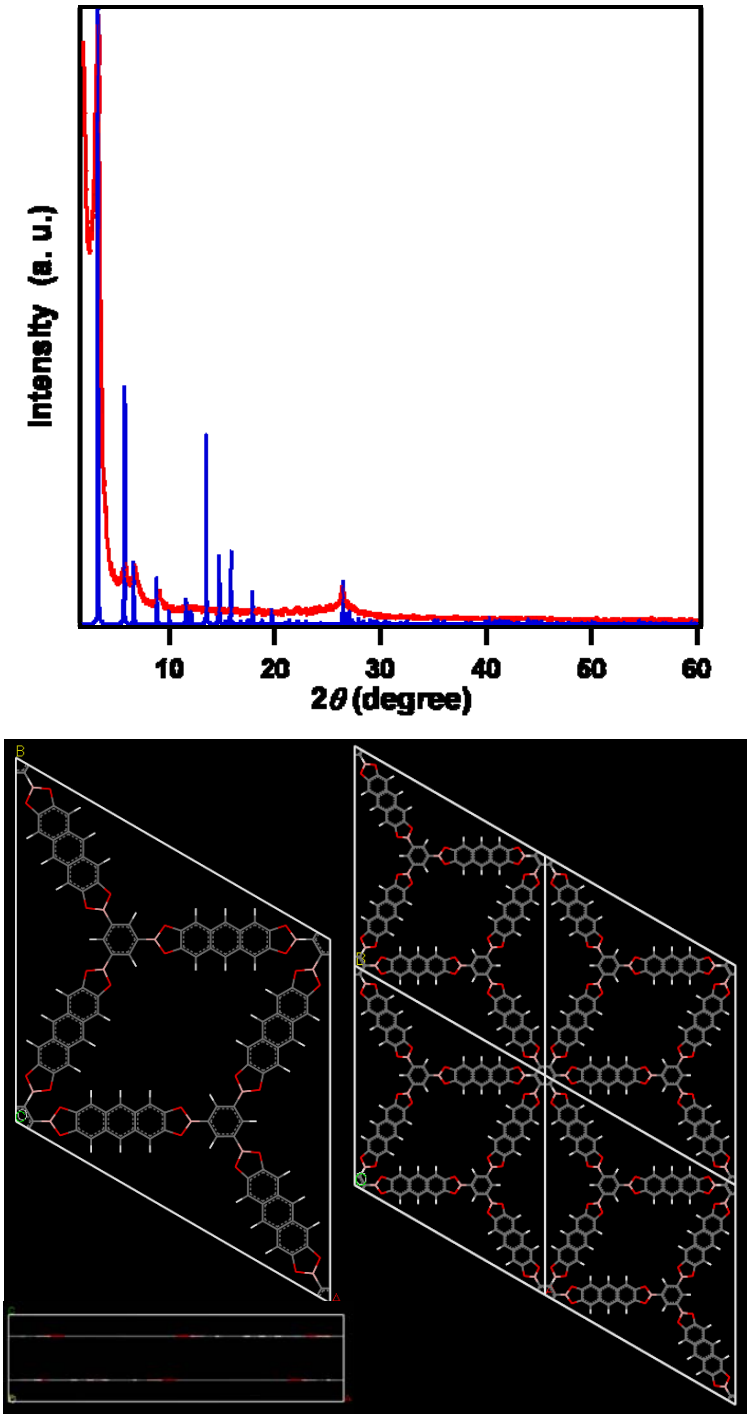

Figure 4-9.PXRD pattern of An-COF and simulation of crystal lattice packing in the staggered form. In the upper figure, the red curve represents the experimental PXRD pattern and the blue pattern is calculated from the staggered crystal packing (Crystal space group *P*63/mmc; No. 194). The simulated pattern does not fit the experimental data at all. The lower figure shows the staggered

crystal lattice packing. In this case, the pore is covered and the pore size is significantly smaller than the experimental one.

Nitrogen Sorption Isotherm Measurement

We carried out nitrogen sorption isotherm measurement to investigate the porosity of An-COF. As shown in Figure 4-10a, An-COF exhibits a typical type IV nitrogen sorption curve, indicative of a mesoporous character[4]. BET calculation gives specific surface area and pore volume of 456 m^2 g^{-1} and 0.4605 cm^3 g^{-1}, respectively. Estimation of pore size with the DFT model shows a diameter of 2.6 nm (Figure 4-10b), which is close to the theoretical one. Pore distribution profile exhibits that in An-COF the specific surface area originates predominately from the persistent mesopores, whereas contribution of other pores formed between sheets or from defects are small (Figure 4-10b). All the above results indicate that An-COF is a crystalline material with a uniformly sized mesopore formed via the eclipsed packing of the polymeric sheets.

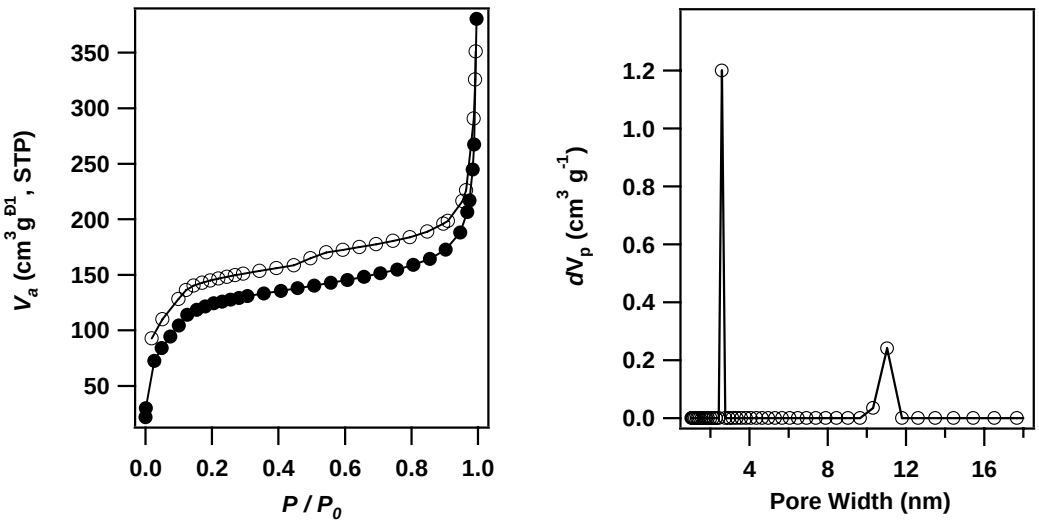

Figure 4-10.(a) Nitrogen adsorption (●) and desorption (○) isotherm profiles of An-COF at 77 K. (b) Pore size distribution of An-COF by DFT modeling on the N_2 adsorption isotherms.

Fluorescence Spectral Profiles

Fluorescence microscopy exhibits that the belts of An-COF are blue luminescent (Figure 4-11a). Condensed poly(boronate ester)s bearing fluorene units have been reported to be blue-emissive materials[5,6]. Fluorescence spectroscopy shows that An-COF emitted a luminescence at 429 nm, upon excitation of the anthracene units at 340 nm (Figure 4-11b, red curve).

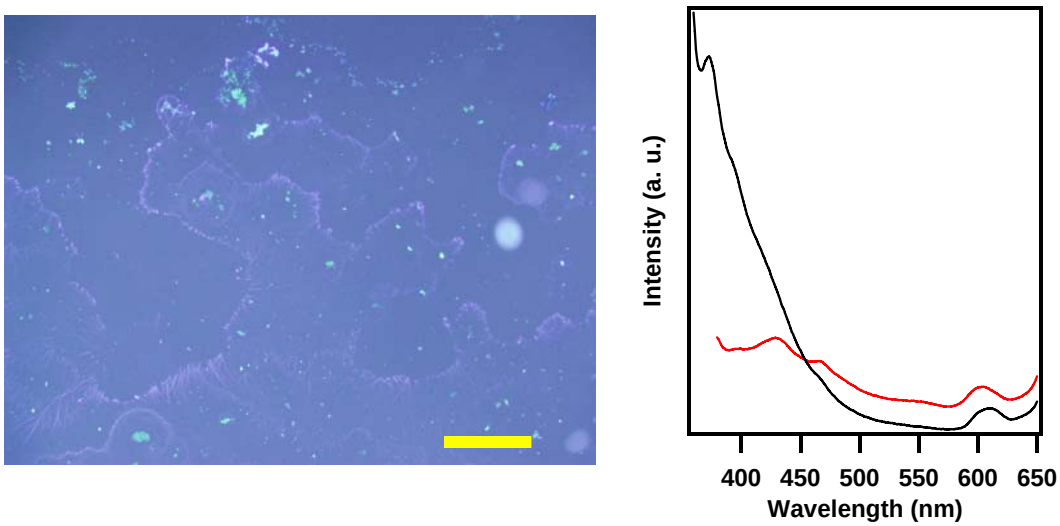

Figure 4-11.(a) Fluorescence image of An-COF. (b) Normalized fluorescence spectra of An-COF (red curve) and mixture of BTBA and THA (black curve) upon excitation at 340 nm at 25 °C.

We also measured the excitation spectrum with diffuse reflectance UV-Vis spectrum of An-COF (Kubelka-Munk spectrum; shown in Fig. 4-12b).

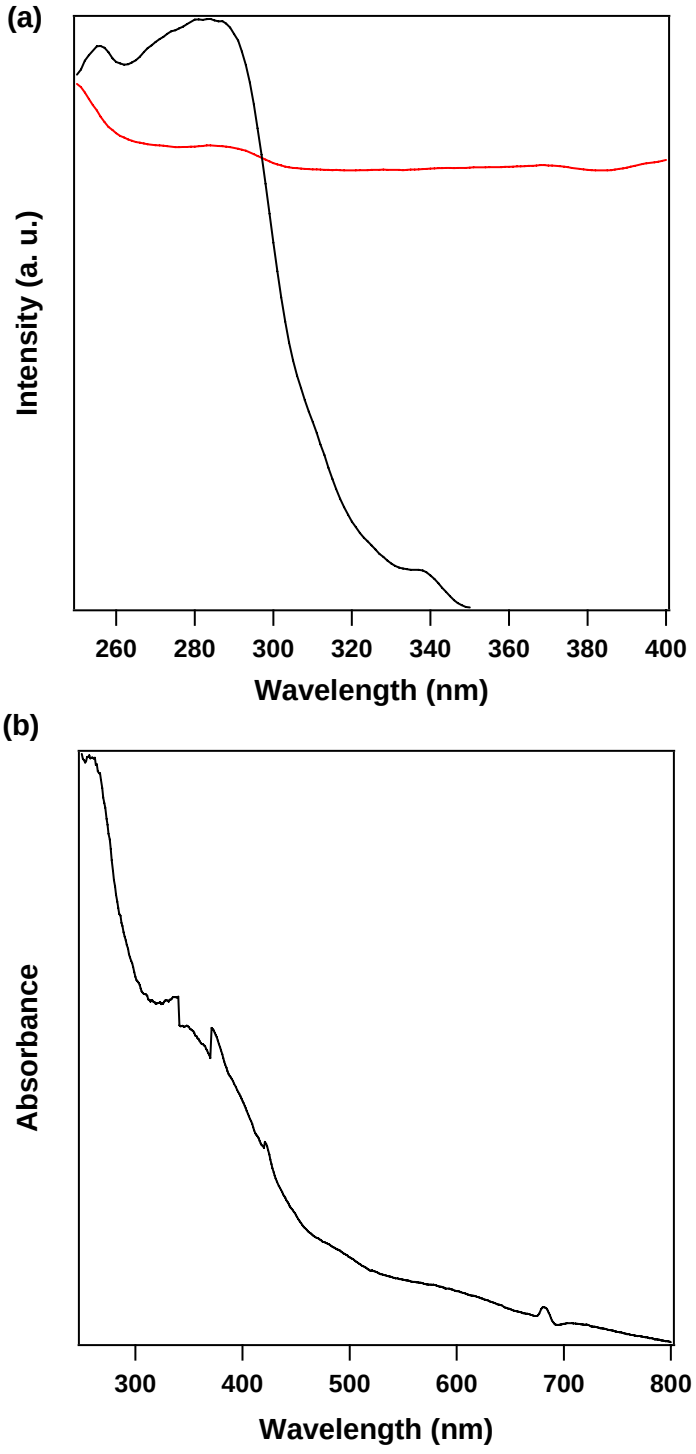

Figure 4-12.(a) Normalized fluorescence excitation spectra of mixture of BTBA and THA (black curve)and An-COF (red curve). (b) Diffuse reflectance UV-VIS-NIR spectrum of An-COF.

Fluorescence Anisotropy of An-COF

Along this line, we further investigated the fluorescence anisotropy of An-COF upon excitation with a polarized light. When a chromophore with a restricted Brownian motion is excited by a polarized light, it emits a polarized fluorescence. However, the fluorescence should be depolarized when the excitation energy migrates randomly within the lifetime of the excited state. Here, fluorescence anisotropy (p) is defined by $(I_{||} - GI_{\perp})/(I_{||} + GI_{\perp})$, where $I_{||}$ and $I_{\perp}$ are fluorescence intensities of parallel and perpendicular components relative to the polarity of the excitation light, respectively, where G is an instrumental correction factor. The 3:2 solid mixture of THA and BTBA shows a p value of 0.002. In contrast, An-COF under identical conditions exhibited a depolarized fluorescence with a p value of 0.628. This observation reveals that An-COF only can mediate energy transfer between components; it cannot facilitate energy migration over the crystalline sheet.

Semiconducting Property of An-COF

Due to the ultimate π-stacking of these large π-conjugated components, An-COF may have a high probability of becoming electrically semiconductive. We investigated this possibility by measuring the electric conductivity with a 10-μm width Pt gap using a two-probe method. An-COF in air at 25 °C shows an almost linear I-V profile (Figure 4-13a, blue curve), while the gap itself is silent irrespective of voltage bias (black curve). For example, at 2-V bias voltage, the electric current is 0.47 nA (Figure 4-13b). In contrast, a 3:2 mixture of THA and BTBA shows a low current (36 pA) under

otherwise identical conditions. Moreover, the electric current can be on/off switched repeatedly for many times without significant deterioration (Figure 4-13b). The relatively high electric current observed for An-COF is likely related to the highly order structure that enables the formation of a conductive path. Upon doping with iodine, the electric current was increased (Figure 4-13a, red curve), suggesting a *p*-type semiconductor character of An-COF.

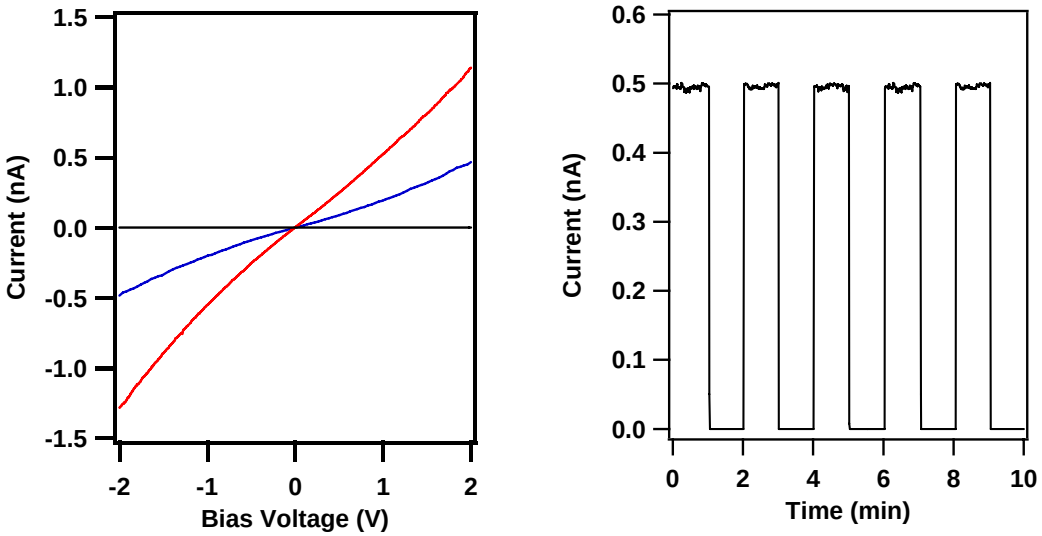

Figure 4-13.(a) I-V profile of An-COF between a 10-μm width Pt gap (black curve: without An-COF; blue curve: with An-COF; red curve: with iodine-doped An-COF). (b) Electric current when 2-V bias voltage is turned on or off.

Photoconductivity of An-COF

We also investigated the photoconductivity of An-COF. An-COF shows a quick response to visible light irradiation (> 400 nm) and displays a linear I-V profile (Figure 4-14). It is noticed that the photocurrent can be repetitively on-off switched for many times with a ratio as 2×10^3 (Figure 4-14b).

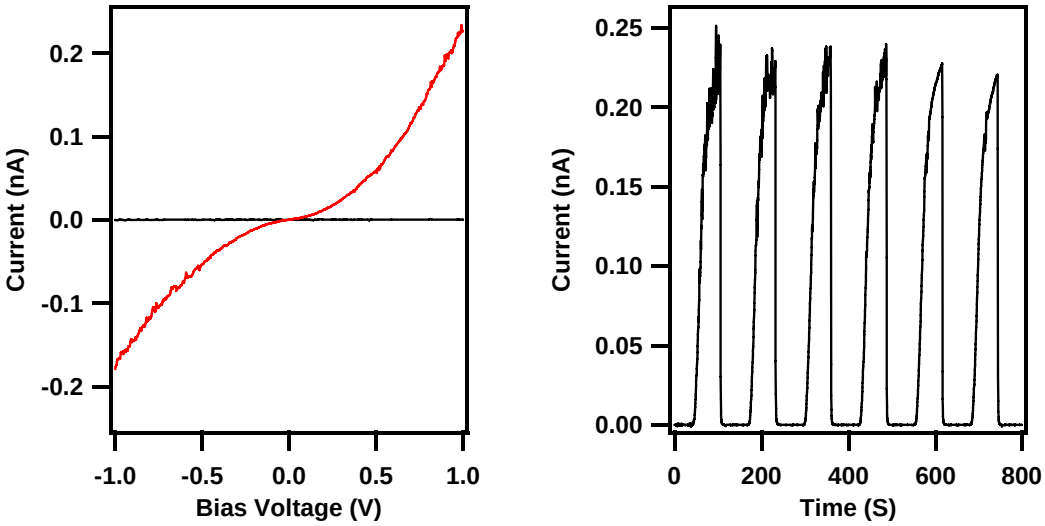

Figure 4-14.(a) I-V profile of An-COF between sandwich type Al/Au electrodes (black curve: without light irradiation; red curve: upon light irradiation). (b) Photocurrent when light is turned on or off.

Crosslink of An-COF

Because of the ultimate alignment of An-COF sheets in a perfectly eclipsed fashion, so it has big possibility to allow photo-induced dimerization[7]. From UV-Vis-IR diffuse reflectance spectrum we found that peak in 250 nm decreased indicate the dimerization of two anthracene units in An-COF (Fig. 4-15).

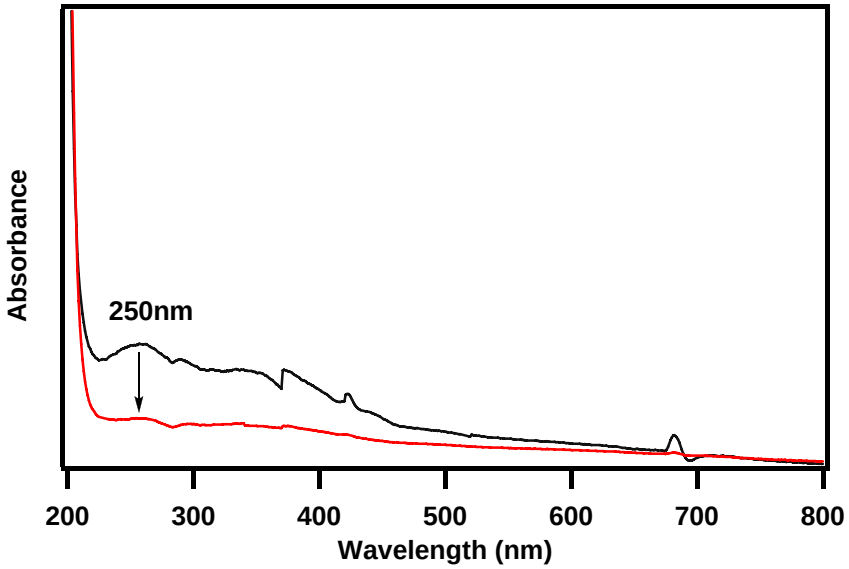

Figure 4-15. Normalized Diffuse reflectance UV-VIS-NIR spectrum of An-COF (black curve) and An-COF after 5h irradiation under 340nm UV light (red curve).

4-4. Conclusion

Exploration of functional COFs is a subject with a high probability to the development of new materials. In summary, we have reported the synthesis of a new COF based on the condensation reaction of benzene and anthracene monomers. An-COF is blue luminescent. Furthermore, An-COF is electrically conductive and capable of repetitive on-off current switching at room temperature. These characters are unique and clearly originate from the highly ordered structure of An-COF.

4-5. Experimental Section

Materials

THF was distilled over benzophenoneketyl under argon before use. Acetaldehyde, anhydrous 1,4-dioxane (99.8%) and anhydrous acetone (99.8%) were purchased from Wako Chemicals. Mesitylene (98%) was purchased from TCI. Veratrol was purchased from Aldrich. Hydrosulfric acid and hydrochloric acid were purchased from Kanto Co. Ltd. Silica gel Wakogel C–300HG was used for column chromatography. Deuterated solvents for NMR measurements were obtained from Cambridge Isotope Laboratories, Inc. BTBA[8-9], THA[10-12] and all the intermediates were prepared according to reported methods (Scheme. 4-1).

Synthesis

All reactions were performed under argon using Schlenk line technique.

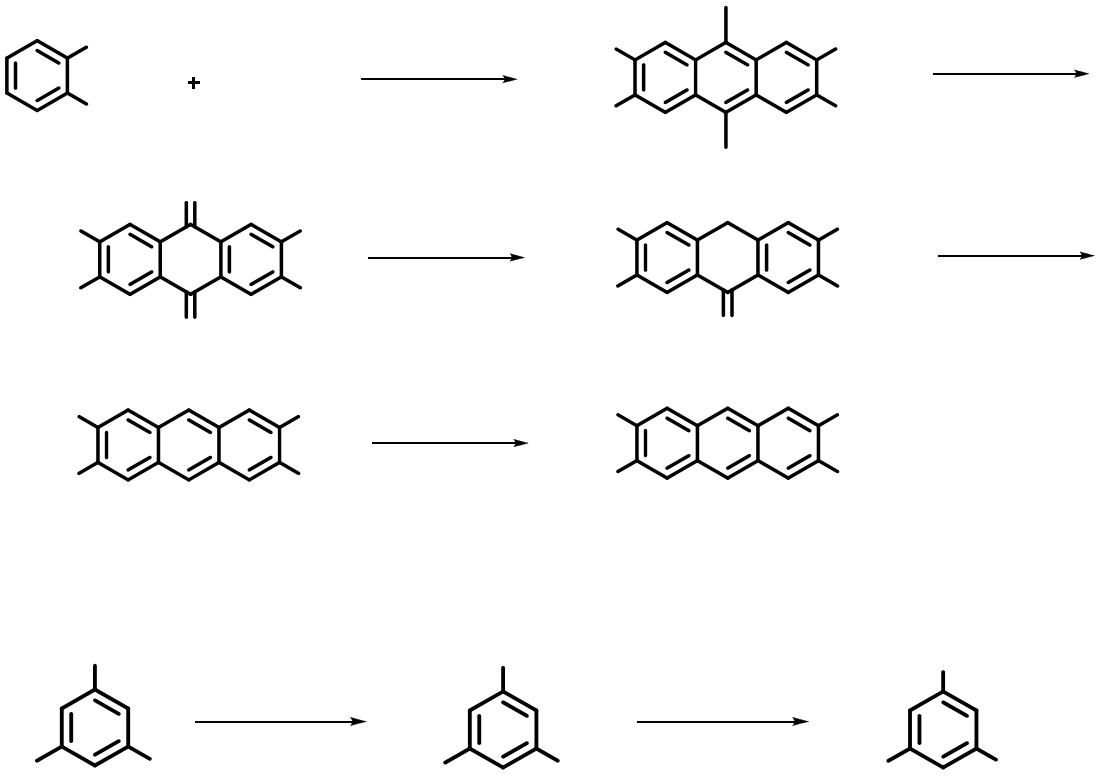

An-COF: THA (24.3 mg, 0.1mmol) and BTBA (17.5 mg, 0.066mmol) were mixed in 1,4-dioxane/mesitylene (1.5mL/1.5mL) in a 10-mL pyrex tube was degassed by three freeze-pump-thaw cycles. Then the tube was sealed, kept in autoclave and heated at 120 °C for 3 days[1]. The precipitate was collected by centrifugation, washed with anhydrous acetone, and dried at 150 °C under vacuum to give An-COF (31 mg) as a green black powder in 81% yield.

Measurements

^{1}H and ^{13}C NMR spectra were recorded on JEOL models JNM–LA400 or JNM–LA500 NMR spectrometers, where chemical shifts (δ in ppm) were determined with a residual proton of the solvent as standard. Infrared (IR) spectra were recorded on a JASCO model FT IR–6100 Fourier transform infrared spectrometer. UV-Vis-IR diffuse reflectance spectrum (Kubelka-Munk spectrum) was recorded on a JASCO model V-670 spectrometer equipped with integration sphere model IJN-727. Matrix–assisted laser desorption ionizationtime–of–flight mass (MALDI–TOF–MS) spectra were recorded on an Applied Biosystems BioSpectrometry model Voyager–DE–STR spectrometer in reflector or linear mode using 9–nitroanthracene or dithranol as matrix. Field emission scanning electron microscopy (FE SEM) was performed on a JEOL model JSM–6700 FE–SEM operating at an accelerating voltage of 1.5 or 5.0 kV. The sample was prepared by drop–casting an acetone suspension onto mica substrate and then coated with gold. Transmission Electron Microscope (TEM) images were obtained on a JEOL model JEM–3200 microscope. The sample was

prepared by drop–casting an acetone suspension of An-COF onto a copper grid. Powder X–ray diffraction (PXRD) data were recorded on a Rigaku model RINT UltimaIII diffractometer by depositing powder on glass substrate, from 2θ = 1.5° up to 60° with 0.02° increment at 25°C.

Geometry optimization of the unit pore structure was performed at PM3 level by using the Gaussian 03 program package (Revision C.02)[2] to give the pore size of 2.6 nm in diameter. Geometry optimization of the repeating unit was performed at B3LYP/6-31G(d) level by using the Gaussian 03 program package in order to make unit cell structure. The final molecular structure in a hexagonal unit cell was prepared by using geometrical parameters from the optimized structure. Molecular modeling and Pawley refinement were carried out using Reflex, a software package for crystal determination from PXRD pattern, implemented in MS modeling ver 4.2 (Accelrys Inc.)[3]. Unit cell dimension was first manually determined from the observed PXRD peak positions by using hexagonal arrangement. We performed Pawley refinement to optimize the lattice parameters iteratively until the RWP value converges. The refinement indicates a hexagonal crystal system with a unit cell of $a = b = 30.3077$ Å and $c = 3.3577$ Å. The pseudo-Voigt profile function was used for whole profile fitting and Berrar-Baldinozzi function was used for asymmetry correction during the refinement processes. Simulated PXRD patterns were calculated from the refined unit cell and compared with the experimentally observed patterns. This structure could have two distinct arrangements: (1) a staggered AB type arrangement with graphite-like packing, where three-connected vertices lie over the center of the six-membered rings

of neighboring layers; (2) an eclipsed AA type arrangement, where all atoms in an each layer of the framework lie exactly over one another. The AA type arrangement was constructed in space group *P*6 symmetry (space group number 191) and the AB type arrangement was constructed in space group *P*63/mmc symmetry (space group number 194). The atoms are placed on the special position to form the 2D framework where all bond lengths and angles are taken from the optimized geometrical parameters calculated at B3LYP/6-31G(d) to maintain reasonable values. After comparing each simulated pattern with experimentally observed pattern, only the simulated pattern from the eclipsed AA type arrangement shows good agreement with the observed PXRD pattern.

Nitrogen sorption isotherms were measured at 77 K with a Bel Japan Inc. model BELSORP-mini II analyzer. Before measurement, the samples were degassed in vacuum at 200 °C for more than 6h. The Brunauer-Emmett-Teller (BET) method was utilized to calculate the specific surface areas. By using density functional theory (DFT) model, the pore volume was derived from the sorption curve.

Electrical measurements were carried out at 25 °C in air on An-COF or I_2-doped An-COF between 10-μm width Pt electrodes by a two-probe method using a Keithley model 2635 source meter. An-COF was homogenously dispersed in acetone and casted onto the electrode to give a film. For I_2 doping, the An-COF electrode was put into an I_2 atmosphere for 1h before measurement. As for the fabrication of devices for photo irradiation, An-COF was dispersed in PMMA/CH_2Cl_2 (An-COF/PMMA = 50/50 wt%) to cast a thin film on Al electrode and Au electrode (30-nm thickness) was vapor

deposited on the top of the film, to give a sandwich-type electrode gaps. PMMA was utilized as a glue to disperse An-COF homogenously since PMMA is free of any absorption in the irradiation wavelength region and has been widely utilized as standard glue for polymer samples in photo-generated carrier conductivity measurement[13]. The film thickness was about 100 μm as estimated by FE SEM measurement. A Xenon light source of Asahi Spectra MAX-301 model was utilized for the irradiation on the top of Au electrode. Due to the difference in electrode configurations, the observed currents are not comparable for those using Pt gap electrodes and sandwich-type Al/Au electrodes.

4-6. References

1. A. P.Côté, H. M. El-Kaderi, H. Furukawa, J. R. Hunt, O. M. Yaghi, *J. Am. Chem. Soc.*,**2007**, *129*, 12914-12915.
2. Gaussian 03, Revision C.02, Frisch, M. J.; Trucks, G. W.; Schlegel, H. B.; Scuseria, G. E.; Robb, M. A.; Cheeseman, J. R.; Montgomery, Jr., J. A.; Vreven, T.; Kudin, K. N.; Burant, J. C.; Millam, J. M.; Iyengar, S. S.; Tomasi, J.; Barone, V.; Mennucci, B.; Cossi, M.; Scalmani, G.; Rega, N.; Petersson, G. A.; Nakatsuji, H.; Hada, M.; Ehara, M.; Toyota, K.; Fukuda, R.; Hasegawa, J.; Ishida, M.; Nakajima, T.; Honda, Y.; Kitao, O.; Nakai, H.; Klene, M.; Li, X.; Knox, J. E.; Hratchian, H. P.; Cross, J. B.; Bakken, V.; Adamo, C.; Jaramillo, J.; Gomperts, R.; Stratmann, R. E.; Yazyev, O.; Austin, A. J.; Cammi, R.; Pomelli, C.; Ochterski, J. W.; Ayala, P. Y.; Morokuma, K.; Voth, G. A.; Salvador, P.; Dannenberg, J. J.; Zakrzewski, V. G.; Dapprich, S.;

Daniels, A. D.; Strain, M. C.; Farkas, O.; Malick, D. K.; Rabuck, A. D.; Raghavachari, K.; Foresman, J. B.; Ortiz, J. V.; Cui, Q.; Baboul, A. G.; Clifford, S.; Cioslowski, J.; Stefanov, B. B.; Liu, G.; Liashenko, A.; Piskorz, P.; Komaromi, I.; Martin, R. L.; Fox, D. J.; Keith, T.; Al-Laham, M. A.; Peng, C. Y.; Nanayakkara, A.; Challacombe, M.; Gill, P. M. W.; Johnson, B.; Chen, W.; Wong, M. W.; Gonzalez, C.; and Pople, J. A.; Gaussian, Inc., Wallingford CT, 2004.

3. Accelrys, Material Studio Release Notes, Release 4.2, Accelrys Software, San Diego 2006.
4. K. M. Sing, D. H. Everett, R. A. W. Haul, L. Moscou, R. A. Pierotti, J. Rouquerol, T. Siemieniewska, *Pure & Appl. Chem.***1985**, *57*, 603-619.
5. W. Niu, M. D. Smith, J. J. Lavigne, *J. Am. Chem. Soc.* **2006**, *128*, 16466-16467.
6. Y. Li, J. Ding, M, Day, Y. Tao, J. Lu, M. D'iorio, *Chem. Mater.* **2007**, *16*, 4600-4609.
7. G. W. Breton, X. Vang, *J. Chem. Educ* **1998**, *75*, 81-82.
8. P. Boudjouk, C. A, Kapfer, *J. Organom. Chem.*, 1985, *31*, 339-348.
9. R. W. Tilford, W. R.Gemmill, H. C. zur Loye, J. J. Lavigne, *Chem. Mater.* **2006**, *18*, 5296-5301.
10. A. Muller, M. Raltschewa, M. Papp, *Chem. Ber.*, **1942**, *75*, 692-703.
11. J. Cason, L. F. Fieser, *J. Am. Chem. Soc.* **1940**, *62*, 2681-2687.
12. Q. Miao, T-Q. Nguyen, T. Someya, G. B. Blanchet, C. Nuckolls, *J. Am. Chem. Soc.* **2003**, *125*, 10284-10287.

13. A. Acharya, S. Seki, Y. Koizumi, A. Saeki, and S. Tagawa, *J. Phys. Chem. B* **2005**, 109, 20174-20179.

Chapter 5

Summary and Perspectives

In **Chapter 2**, the author reported the first example of a luminescent and semiconducting COF, which adopts a belt shape and consists of pyrene and triphenylene functionalities alternatively linked in a mesoporous hexagonal skeleton. TP-COF based on π electron system was synthesized by condensation polymerization with triphenylene and pyrene derivatives as monomers. TP-COF adopts belt morphology. When triphenylene and pyrene units were selectively excited by ultraviolet and visible lights, TP-COF displays strong blue fluorescence, as a result of an efficient energy transfer between two units. This result demonstrates that TP-COF collects photons of a wide range covering from ultraviolet to the visible regions and converts them to blue emission efficiently. In addition, due to the ultimate π stacking of large π-conjugated components, TP-COF is electrically semiconducting. The electric current can be repetitively on/off switched without any deterioration. Upon doping with iodine, the electric current was increased remarkably, which suggests that TP-COF is *p*-type semiconductor.

In **Chapter 3**, the author demonstrated the synthesis of a new π-electronic COF based on self-condensation of pyrene diboronic acid under solvothermal condition (PPy-COF). FE SEM shows that PPy-COF assumes micrometer-sized cubic shape, while no any other morphology such as belt, fiber, sphere, or rod are present, indicating high phase uniformity. PPy-COF exhibits high blue luminescence upon excitation at pyrene unit. PPy-COF is electrically semiconducting and shows *p*-type character. Moreover, the ultimate alignment of 2D poly(pyrene) sheets in a perfectly eclipsed

fashion allows a large charge carrier mobility. High luminescence and large charge carrier mobility are two key parameters in optoelectronics but usually incompatible with each other. In this sense, the combination of high luminescence and large carrier mobility in a single macromolecule is unique and would appeal to well applications in optoelectronics.

In **Chapter 4**, the author disclosed the design and synthesis of a new type of COF based on co-condensation of benzene triboronic acid and 2,3,6,7-tetrahydroxyanthracene under solvothermal or reflux conditions (An-COF). An-COF consists of benzene and anthracene components alternatively linked in a mesoporous hexagonal skeleton. FE SEM reveals that An-COF adopts well-defined micrometer-scaled 2D sheet shape. Moreover, An-COF is electrically semiconducting and highly luminescent. The ultimate alignment of An-COF sheets in a perfectly eclipsed fashion allows photoinduced dimerization and reversible monomerization of anthracence units in An-COF. Such a photo-addressable COF may find applications in tuning luminescence and high-density data storage.

Exploration of functional COFs is a subject that has a high probability to lead to the development of new materials.

In summary, the author has developed a series of novel π-electronic sheet-shaped macromolecules and covalent organic frameworks. Based on the chemistry of boronic ester formation reaction, the author designed and synthesized a series of new π-electronic monomers and succeeded in the construction of π-electronic sheet-shaped

macromolecules. By using different monomers and polymerization methods, 1D belt-shaped (TP-COF), 2D sheet-like (An-COF) and 3D cubic (PPy-COF) COFs were created. These π-electronic organic frameworks show unique photo and electrical functions that clearly originate from their highly ordered structures and thus open a new way to polymeric optoelectronics and electronics.

List of Publications

1. Shun Wan, Jia Guo, Jangbae Kim, Hyotcherl Ihee, Donglin Jiang
   "A Belt-Shaped Blue Luminescent, and Semi-conducting Covalent Organic Frameworks"
   Angew. Chem. Int. Ed., **2008**, 47, 8826-8830 (VIP and selected as a frontispiece of ACIE). Highlighted by *C & EN*, **2008**, *86*, 29. "Covalent Conducting Belts".

2. Shun Wan, Jia Guo, Jangbae Kim, Hyotcherl Ihee, Donglin Jiang
   "Towards Photoconductive Covalent Organic Framework: Self-Condensed Arene Cubes with Order of 2D Polypyrene Sheets for Prominent Photocurrent Generation"
   Angew. Chem. Int. Ed., **2008**, *Accepted*.

3. Shun Wan, Jia Guo, Jangbae Kim, Hyotcherl Ihee, Donglin Jiang
   "A light-Driven Shape-Tunable Covalent Organic Framework"
   In Preparation.

Acknowledgement

This thesis could not be finished without the help and support of many people who are gratefully acknowledged here.

At the very first, I'm honored to express my deepest gratitude to my dedicated supervisor, Prof. Donglin Jiang, with whose able guidance I could have worked out this thesis. He has offered me valuable ideas, suggestions and criticisms with his profound knowledge in chemistry and rich research experience. His patience and kindness are greatly appreciated. Besides, he always puts high priority on our dissertation writing and is willing to discuss with me anytime he is available. I have learnt from him a lot not only about dissertation writing, but also the professional ethics. I'm very much obliged to his efforts of helping me complete the dissertation.

I owe special thanks to our assistant professor Dr. Tomoya Ishizuka for his priceless contributions on this study. He also encouraged me to become a responsible academic, helped me identify the strengths and weaknesses associated with different research approaches.

I'm also extremely grateful to our JSPS postdoc, Dr. Jia Guo, whose patient and meticulous guidance and invaluable contributions are indispensable to the completion of this thesis. I cannot make it without his support and encouragement. The most important point, he provided me honest and reliable friendship.

In regards to my group collaborations, I would like to thank those that have helped expand my research repertoire.

What’s more, I wish to extend my thanks to Prof. Dr. Hyotcherl Ihee and Mr. Jangbae Kim in KAIST, Republic of Korea, for their hard working for stimulation parts of my thesis.

Thanks are also due to my friends, who never failed to give me great encouragement and suggestions. Special thanks should go to Miss. Tan Xu, Dr. Feng Su, Mr. Ji Zhou, and Mr. Lanfan Zhang Miss Junjun Li for their encouraging me when I had any kind of problems in my research and daily life.

At last but certainly not least, I would like to thank my parents for their unconditional support, understanding, and dedication all the way from the very beginning of my Ph.D study. I am thankful to all my family members for their thoughtfulness and encouragement.